Final Report

Modeling the Interface Between a Respirator and the Human Face

Dino Piccione
Dr. E. Thomas Moyer Jr.

COTR: Kathryn S. Cohen

Prepared for:

Contract No. DAAL01-96-C-0077
Army Research Laboratory
Human Engineering and Research Directorate
Aberdeen Proving Ground, Maryland 21005

Prepared by:

DCS Corporation
1330 Braddock Place
Alexandria, VA 22314

March 15, 1997

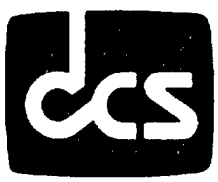

REPORT DOCUMENTATION PAGE

Form Approved
OMB No. 0704-0188

1. AGENCY USE ONLY *(Leave blank)*	2. REPORT DATE	3. REPORT TYPE AND DATES COVERED
	15 March 1997	Final Report

4. TITLE AND SUBTITLE
Modeling the Interface Between A Respirator and the Human Face

5. FUNDING NUMBERS
Contract No. DAAL01-96-C-0077

6. AUTHOR(S)
Dino Piccione
E. Thomas Moyer, Jr.

7. PERFORMING ORGANIZATION NAME(S) AND ADDRESS(ES)
DCS Corporation
1330 Braddock Place
Alexandria, VA 22314

8. PERFORMING ORGANIZATION REPORT NUMBER

9. SPONSORING/MONITORING AGENCY NAME(S) AND ADDRESS(ES)
Army Research Laboratory
Human Research and Engineering Directorate
Attn: AMSRL-HR-MM (K. Cohen)
Aberdeen Proving Ground, MD 21005-5425

10. SPONSORING/MONITORING AGENCY REPORT NUMBER

11. SUPPLEMENTARY NOTES
Prepared in Response to SBIR Solicitation 95.3 (Phase I)

12a. DISTRIBUTION AVAILABILITY STATEMENT
Approved for public release; distribution is unlimited

12b. DISTRIBUTION CODE
A

13. ABSTRACT *(Maximum 200 words)*

Report developed under SBIR contract.This report documents a multi-disciplined approach to the issue of modeling the interface between the respirator (protective mask) and human face. The modeling efforts encompass discomfort, digital modeling of mask surfaces, digital modeling of the human face, and finite element analysis (FEA). The FEA process was used to register the digital model of the mask seal onto the digital model of a face. The finite element modeling evaluated the boundary conditions to predict fit and discomfort.

14. SUBJECT TERMS
Protective Mask
Finite Element Analysis
Discomfort
Human Factors
Computer-Aided Design
SSBIR Report

15. NUMBER OF PAGES
50

16. PRICE CODE

17. SECURITY CLASSIFICATION OF REPORT	18. SECURITY CLASSIFICATION OF THIS PAGE	19. SECURITY CLASSIFICATION OF ABSTRACT	20. LIMITATION OF ABSTRACT
Unclassified	Unclassified	Unclassified	UL

Final Report

Modeling the Interface Between a Respirator and the Human Face

Dino Piccione
Dr. E. Thomas Moyer Jr.

COTR: Kathryn S. Cohen

Prepared for:

Contract No. DAAL01-96-C-0077
Army Research Laboratory
Human Engineering and Research Directorate
Aberdeen Proving Ground, Maryland 21005

Prepared by:

DCS Corporation
1330 Braddock Place
Alexandria, VA 22314

March 15, 1997

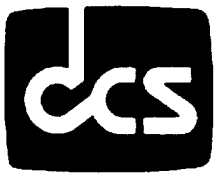

Table of Contents

1.0 Introduction

This technical report covers the work that was performed as part of the Department of Defense Small Business Innovation Research (SBIR) program solicitation 95.3. The topic addressed the development of graphical and mathematical models of the M40 protective mask, the human face and the interrelationship between protective mask and face when the mask is worn. The purpose of this Phase I project is to determine the technical feasibility of a proposed concept which involves the use of a discomfort model, finite element analysis, laser scanning, and computer aided design tools to perform the protective mask design task.

The objectives of this SBIR program centered on the problem of the number of iterations required to complete the mask design process. The design of a mask requires many iterations to check that the final product meets the set of requirements to satisfy operational needs, provides the required level of protection, and can be produced at the target cost. The overarching objective of any Phase I SBIR project is to determine the feasibility of the concept and lead to the development of a well defined product during Phase II. The focus of this SBIR was to determine the feasibility of developing a method for evaluating the interface between a respirator and the human face. The objectives were to develop graphical and mathematical models of the M40 protective mask, the human face, and the interrelationship between protective mask and face when the mask is worn. The development included predictive techniques for estimating the levels of comfort and protection provided by a mask prior to fabrication of prototypes. To perform these predictions and perform iterative evaluations of a mask design will require the design, fit, and evaluation process to be performed in a virtual environment. This SBIR project has developed the required models to determine the feasibility of developing a system of models that will perform this function.

The development of a protective mask or respirator is a difficult and challenging task. The mask must provide the requisite degree of protection from chemical and biological agents while allowing the user to perform tasks required to complete the mission. The method used to address this issue during Phase I was to search the literature for data on this topic and demonstrate the use of finite element analysis (FEA) to model and evaluate the mechanical conditions at the interface between face and mask. The use of 3D laser scanning technology and computer aided design (CAD) software were integrated as part of this effort as a means of generating computer files that model the surfaces of the mask and a face. The overall objective has been to address the feasibility of performing fit and comfort evaluations during the mask design process without the need for constructing a physical model of the mask. Such a process would reduce the dependence on the requirement to build physical prototypes and mock-ups.

In the sections below we will discuss the feasibility of this concept and how it relates to the mask design process.

2.0 Literature reviews

2.1 Mask-induced discomfort

The role of mask forces on the head and face

The Phase I effort to model the mask/face boundary relied in part on performing literature searches to uncover previous work containing quantifiable results that can provide the basis for elements of the model. A central issue that guided the literature search was that the model needs to address the mechanical aspects of comfort that can be analyzed and adjusted. The first point that must be made is that while the term "comfort" is often used in the context of an effect of mask fit, the real parameter with which we must be concerned is "discomfort". Discomfort is clinically termed dysesthesia (an unpleasant abnormal sensation, whether spontaneous or evoked). In common parlance, "comfort" may refer to both comfort and discomfort. Comfort cannot be a meaningful design criterion unless referenced to its operational task requirements (Lueder, 1983). The results of the literature review and the experience of the research team points toward the concept that discomfort and comfort are very different entities. Discomfort is primarily associated with physiological and biomechanical factors and comfort is primarily associated with aesthetics (Zhang, Helander, & Drury, 1996). The focus of this portion of the research effort is on the effect of mask design on discomfort.

From the standpoint of sensation, discomfort has varying levels. The extreme regions of discomfort are classified as pain. Pain is defined as an unpleasant sensory and emotional experience associated with actual or potential tissue damage, or described in terms of such damage (International Association for the Study of Pain, 1994). We must dismiss comfort as a design requirement in favor of specifying that a respirator must not cause discomfort, pain, or tissue damage under operational conditions after a specified period of time. Several of the design handbooks and test documents reviewed during this project have noted that comfort is subjective and difficult to quantify. However, the results of this literature search indicate that evaluating discomfort using physiological measures and verifiable descriptors on rating scales may be achievable (Zhang, et al (1996).

An effort was made to determine the characteristics of the sensory and perceptual mechanisms that play an important role in the issue of discomfort due to equipment mounted on the head and face. With the exception of pain related to heat, very little helpful literature was found that investigates the exact nature of the pressure and pain sensory organs. The literature focuses more on the nature of the afferent nerve fibers connected to the nerve endings. Some of the literature argues with the concept that specific receptors linked via pathways to the brain centers are responsible for specific sensations (Rollman, 1991). Rather than using a simplistic specificity theory of pain, it is suggested that perhaps a pattern theory is more accurate. This pattern theory postulates that the stimulus intensity or summation of neural impulses by a central mechanism are the critical determinants of pain.

A third theory of pain is that of the spinal gate control mechanisms (Schiffman, 1990). This theory shows that there is a competitive interaction between two different types of nerve fibers, the fast fibers (Aβ) and slow (Aδ and C). The latter "gate-control" theory currently enjoys the greatest favor in the research community and is supported by the preponderance of experimental data. While this pain theory material helps to form a background for the modeling of the interaction between the human face and a protective mask, there was little that could be directly applied to a model used in the protective mask design process.

The literature search has included research performed by respirator designers and the medical community. There is data that relates mask-induced discomfort to pressure, area, and region of the face as relevant parameters. The medical research that is applicable to this effort is that which is related to the formation of decubitus ulcers known as bed sores. These ulcers are formed as a result of pressure and shear forces as well as friction acting on skin with an underlying bony structure. To place this in a context that has operational relevance to the Army, a technical report from the US Army Aeromedical Research Laboratory (USAARL) reported that during their study of pilots wearing chemical protective equipment the most common reason for failure to complete a "flight day" was injury due to equipment. This was especially true for scalp and face hot spots due to mask fit and wear (Mitchell, Knox, Edwards, Schrimsher, Siering, Stone, and Taylor, 1986). These became significant problems by the third and fourth days. The injuries described and shown in the report bear a striking resemblance to the ulcers shown in the scientific literature on decubitus ulcers reviewed during this Phase I effort.

One of the key pieces of research indicates that the sensation associated with pressure against the face in areas where a respirator would make contact follows Steven's Law (Snook, Hinds, and Burgess, 1966). This is a well established psychophysical function that has been verified in a number of sensory modalities. The specific function for sensing force against the face is:

$$S=aI^{1.29}$$

S = sensation of pressure
a = constant
I = intensity of pressure

The most sensitive areas in the face were the frontal eminence (corner of the forehead) and maxilla frontal process (bridge of the nose). The least sensitive areas were in the area of the sellion (depression at the nasal root), glabella (between the eyebrows), and the frontal bone on the centerline (middle of the forehead). These experimental results correlate well with field experience and operational/developmental test results (Decker & Piccione, 1982). In long-term wear tests, soldiers usually complain of discomfort and pain induced by the mask nosecup on the bridge of the nose and by the mask seal on the forehead (Mitchell, et al, 1986). These are both areas where the mask exerts pressure on the face and the soft tissue is relatively thin and has a bony backing. Other areas of the face have relatively more tissue that can compress and conform in response to the pressure exerted by the mask contact area. The areas with thicker tissue can also react more favorably to the shear forces exerted by the mask. In another study

of forces exerted by mask seals , the equation given above was verified, but with a slightly lower exponent (Burgess, Hinds, and Snook, 1970).

It was noted during the literature search that none of the documents contained the results of experiments that related the physical and physiological aspects of this issue to subjective ratings of discomfort or pain. The experiments that concentrated on very detailed investigations of the effect of physical forces did not ask the experimental subjects to rate the discomfort on a rating scale. The tests and evaluations that rated, or at least reported, discomfort did not have the physiological aspects of the human interface documented. To produce meaningful results, future research should concentrate on the use of a valid and reliable discomfort rating scale coupled with appropriate instrumentation that accurately measures the forces acting on tissue as well as relevant resultant parameters such as skin blood flow.

In this latter study (Burgess, et al., 1970), it was interesting to note that when three respirator facial seal designs were compared, one type required significantly greater strap tension to provide the equivalent degree of protection available with the other seal designs. The study discussion indicated that the inferior seal design had a well defined form and required greater force to permit continuous facial contact. The impact of seating force on leakage is greatest at the lower values. When the data are plotted, the leakage versus seating pressure curve is logarithmic. That is, at low seating forces small increases in force will result in relatively large decreases in leakage. At the higher forces a small increase in force results in a relatively small decrease in leakage. Variations in leakage between masks at low seating forces is believed to be due to differences in the flexibility of the individual facepiece and the resulting ability of the masks to conform to the face. The initial fit achieved with a minimum seating force apparently is a significant indicator of performance since the mask leakage ranks were consistent throughout the entire force range. The data show that adequate seating may be established at moderate seating forces and additional increase in force may not appreciably reduce leakage.

Several definitive studies that were widely cited in the literature addressed the issue of tissue damage and skin blood flow occlusion as a result of pressure, shear, and friction. One study on the etiology of decubitus ulcers performed eighty separate experiments on animals to accurately determine the effect of pressure on skin and muscle (Kosiak, 1960). The data showed that there was a marked susceptibility of tissue to relatively low constant pressures for short periods of time. Pressures as low as 1.35 pounds per square inch (psi) applied for a continuous two hour period were sufficient to show moderate changes in muscle structure. Figure 1 shows the relationship between pressure and period of application when actual tissue damage could be observed. These data indicate that if a mask is to be worn for as long as 12 hours an application of approximately 2 psi of pressure by the seal on the face can be expected to cause tissue damage. The extent of the damage increased as exposure and pressure were increased. Edema and hyperemia (swelling and redness) were usually noted immediately following the release of pressure over the test area, and generally lasted half as long as the duration of the application of pressure. This type of effect has often been observed on soldiers wearing protective masks for extended periods. Kosiak reported that ulcerations were observed after three or four days of experimentation. This coincides with

the USAARL study cited above. Relieving the pressure has been shown to allow recovery of the tissue as long as cell damage is not too extensive.

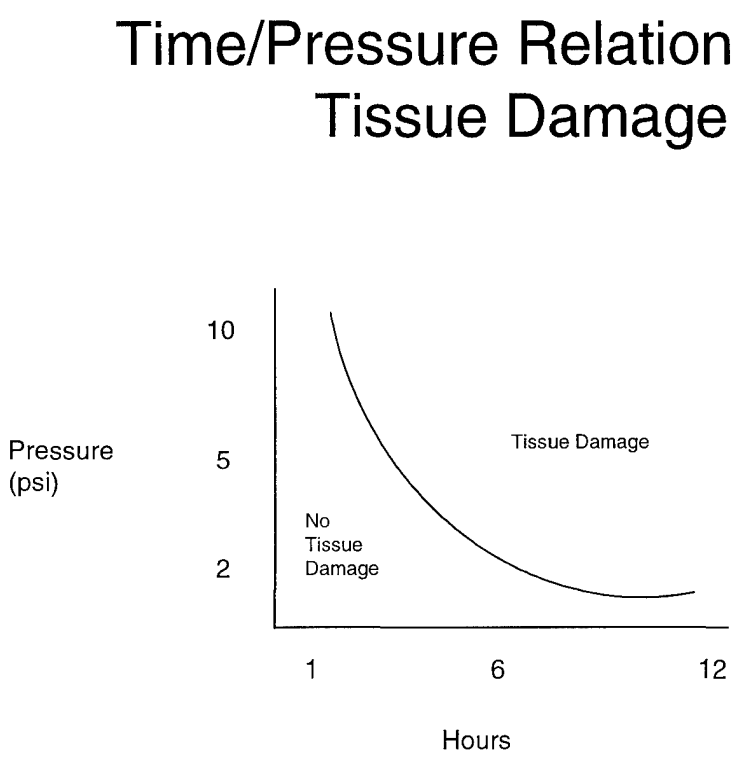

Figure 1. (from Kosiak, 1960)

Skin cell damage is related to blood flow. The level of transmural pressure at which the blood flow stopped was called the "critical closing" pressure. This "critical closing" pressure could be produced either by an increase in externally applied pressure or a decrease in intravascular hydrostatic pressure. What is perhaps of greater importance is that while tissue shows a marked susceptibility to damage at relatively low constant pressures for short periods of time, there was a greater resistance to change following the application of equal amounts of intermittent pressure(Kosiak, 1960). Test conditions of up to 4.6 psi applied for a three hour period showed no damage if the application was intermittent. Continuous applications of pressure at 2.85 psi for a 12-hour period produced cellular changes. Similar damage was seen if the continuous applied force was 9.5 psi for one hour. From a mask design standpoint, it would be beneficial if there was a way to alternate the location of pressure points on the scalp and face when the mask is worn for long periods. When performing testing of respirators, it would appear to be beneficial to measure capillary circulation in the area of pressure points. Such measurements can be made noninvasively using a laser-

Doppler velocitometer (Xakellis, Franz, Arteaga, & Meletiou, 1993). The cessation or slowing of blood flow is an indicator of impending tissue damage.

To study shear versus pressure as causative factors in skin blood flow occlusion, a series of experiments were reviewed that measured (1) pressure alone, and then (2) shear that was increased in steps with the smallest amount of associated pressure (Bennett, Kavner, Lee, and Trainor, 1979). The results of the first set of experiments were compared to earlier studies to assure that the experiment was referenced on the earlier "benchmarks". The overall results showed that at a sufficiently high level of shear (roughly 1.4 psi) the pressure necessary to produce occlusion was half that required when little shear was present. The application of a unit of pressure is equal to 2.6 units of shear in terms of the tendency to restrict arteriole flow and promote occlusion. While pressure is the main determinant of blood flow occlusion, shear is a significant factor and must be analyzed when modeling the contributing factors in discomfort and potential tissue damage.

An additional study that can be cited concerns the role of pressure and friction in the causation of ulcers on the skin (Dinsdale, 1974). This was also a series of animal studies that applied pressure to the skin with and without friction for various periods. The main result of this study was that friction increased the susceptibility to skin ulceration at constant pressures of less than 9.5 psi. Above this value friction had no effect. Friction and repetitive pressure of only 0.86 psi resulted in skin ulceration within 18 hours. The same degree of ulceration was produced within 18 hours by 5.6 psi without friction. The significance of this finding is that this may predict an increase in discomfort when protective masks are worn with helmets in helicopters and combat vehicles. The helmet may increase the level of pressure exerted by the mask on the face and scalp, but the additional mass is vibrating and introduces friction to the head/mask system. The addition of friction as a factor may add to the attack on the skin, and the resulting tissue damage may cause pain.

2.2 Laser scanning and computer aided design

The literature on the use of laser scanning in the design process is increasing on a daily basis. Numerous articles in various trade publications address new applications for laser surface scanning devices and novel approaches to solving problems involving apparel and equipment used by humans. The most relevant and well documented applications involve the Computerized Anthropometric Research and Design (CARD) laboratory at the Fitts Human Engineering Division of Armstrong Laboratories at Wright-Patterson Air Force Base, Ohio. The CARD lab has several publications that document their efforts to improve and automate the design process for protective clothing and equipment. They have developed a method to improve the fit of the Air Force oxygen mask on individuals that are hard to fit to support the Advanced Aircrew Oxygen Mask (AAOM) program (Crew Technology Division of Armstrong Laboratory, 1996). The automated custom mask manufacturing process involves a laser scan of the individual's head to obtain basic contour information. The individual is scanned again wearing a helmet and standard oxygen mask. A third scan with the individual wearing only the best fitting face piece is then made to register the mask on the original scan.

Software developed for the AAOM then creates a new sealing portion of the face piece and saves the new design as a file that is exported to a manufacturing facility. The main contribution of this capability is that it speeds the process and eliminates the need for a plaster cast of the individual.

Several publications sponsored or published by the CARD lab have specified how the use of 3D laser scanning has aided the helmet design process. They have asserted that the old methods of using traditional anthropometric data are not only inadequate, but have contributed to poor design (Whitestone and Robinette, 1996). They have debunked the concept of using reference planes (such as the Frankfort plane) for head measurements. The main problem has been that before the arrival of advanced 3D surface digitizing techniques, designers had little or no surface information pertaining to head alignment. This lack of information on surfaces and the use of linear dimensions lead to the creation of too many sizes to accommodate the variance in the data. The use of the traditional anthropometric data also lead to odd proportions in size and shape. They have indicated that in a test of the HGU-53/P U.S. Air Force aircrew helmet, it was found that only two sizes (one for men and one for women) are required to fit the same percentage of the population as the original set of six sizes. The size intended to be largest was improperly proportioned so that, even though larger in volume than the next smaller size, it did not fit larger heads. The CARD lab publications point toward the use of 3D scanning as the main tool that can help the fit process. They introduce the concept of feature envelopes to aid in the protective equipment design process. Feature envelopes describe the spatial location and orientation of areas of interest (i.e., features) with respect to a well defined, easily duplicated coordinate system. The concept of feature envelopes may have utility in the task of designing protective masks in that the coordinate system could originate at the chin cup and the relative location of important features (pupils, bridge of the nose, hair line, etc.) could be specified. The 3D laser scanner at the CARD lab is used in a novel way by conducting a series of scans with the individual unencumbered, while the individual is wearing the protective equipment, and then a scan of only the equipment. By performing a series of registrations of the different scans and by subtracting and adding elements from the three scans, a composite picture can be formed, as well as "X-ray" views that show how the face fits within the equipment.

The CARD lab has accumulated a library of over 1000 files containing 3D scanned images of heads and faces. The application of these files ranges from custom fitting of oxygen masks to research in helmet fit. The files are available to other government agencies and have been successfully exported in any format requested by their clients. The CARD lab was contacted as part of the effort covered by this report and they have indicated that they are not aware of any research or application that seeks to combine the technologies of CAD, 3D laser scanning, and finite element analysis to aid in the protective equipment design process. They were not aware of any software tools that help a designer with the process of fitting a protective mask to a face in a virtual environment. However, they indicated strong interest in the development of such tools.

It is apparent from a review of the literature that the crew systems and life support equipment community is receptive to the insertion of new tools using digitized 3D forms of the human

face and automated tools that can be used in the design process. In a discussion of the helmet sizing and fitting process Robinette (1993) indicates that the use of digital surface data is too massive in its entirety, but a few relevant contours and important landmarks can be extracted. However, the analytical techniques described in this paper were essentially extensions of existing techniques and advocated the use of human subjects to indicate the presence of pressure points and the acceptability of center of mass and other discomfort parameters. There was a passing reference to the use of advanced analytical methods, including finite element analysis, but these were described as either "experimental" or "classical" and their application to the fit process was not seriously discussed.

A recurring issue in the development of head-mounted equipment is the collection of accurate anthropometric data that identifies relevant anatomical landmarks. The relative location of these landmarks is important to the problem of developing sizing schemes to fit a range of the population. In a discussion of the design and evaluation of helmets, Whitestone (1993) indicates that the high resolution surface scans of heads and the relationship to helmets and other protective equipment can help to match the anatomical landmarks with the equipment interfaces. The most interesting development in this process is shown in a paper on the automatic detection of those landmarks (Geisen, Mason, Houston, Whitestone, McQuiston, and Beattie, 1993). This method advocates the use of anatomical markers (a high contrast "bull's eye" target) as fiduciary landmarks. The laser scan of the anatomical surface will register these markers and software is used to calculate the location of the landmarks in a coordinate system. The system was used to marry the 3D laser scan of limbs to a CAD program for the construction of prosthetics for the Veteran's Administration. A somewhat different approach using an iterative algorithm (Bhatia, Fiehler, Smith, Commean, and Vannier, 1994) has some promise of comparing digitized human anatomy surfaces obtained over extended periods of time. DCS is currently investigating the use of these techniques as a way of registering the position of patients during the process of administering radiation treatments using the DCS 3D Areal Mapping System. This mapping system is briefly described in section 4.0 below.

In a search for organizations using mathematical or graphical models in the process of designing or testing protective masks or respirators, a member of the design team at the Edgewood Research, Development & Engineering Center (ERDEC) was contacted. ERDEC is currently using one of the "high end" CAD applications (CADDS 5, Computervision, Inc.). Mathematical or graphical models are not now in use. An attempt was made to use the ANSYS finite element analysis software in conjunction with the CAD process to analyze the mask-face interface. The attempt was not successful, however, there is an expressed desire to do more modeling so that the design process can be iterative prior to building physical prototypes. Many of the advanced CAD applications such as ProEngineer, AutoCAD, and CATIA, purport to enable finite element modeling, but this is usually a provision in the software that allows an additional FEA application such as ANSYS, ABAQUS, HyperMesh, NASTRAN, etc., to be run using the model in the host software. ERDEC is using the CAD system to generate rapid prototypes. The total prototying process takes several months. The process of designing the seal shape and size is performed using digitized models of mold

cores. The sizing is based on molds from previous respirator designs that fit the specified population.

Cyberware scanners are in use in a plethora of biomechanical applications. They are the "premier" laser scanner to collect anthropometric data, perform research related to biometrics, provide the digital image for special effects in the movie industry, and generate the digital image of patients requiring reconstructive surgery that can be manipulated to review the potential outcome of the surgery. Laser Design scanners are also used in many biometric settings including the fitting of shoes. Other laser scanners used in the biometric environment that were found during this literature search are dedicated to research laboratories or are used in industrial settings to digitize the surface of mechanical parts.

Once an object is scanned by a device the resulting set of points must be analyzed and manipulated to form surfaces and linked to form the digital equivalent of the solid object. Cyberware produces an extensive library of applications that are designed to use the output of their scanning device. Among them are:

- Cymage - polygon reduction software
- Zipper - matches registration points from several scans to form one image
- Cysurf - fits b-splines to the range map
- ntest - surface editor and scan-to-NURBS (non-uniform rational b-splines)
- Cyraw, Cyoptic, Cyview - convert scanner data to SCSI data
- Cytomesh - produces full resolution triangle mesh

Among the tools that are commercially available to perform fit testing of helmets, gloves, and goggles is ShapeAnalysis by Beecher Research Company. This software operates on Silicone Graphics workstations and is compatible with the 3D point data such as those produced by Cyberware laser scanning products. This software purports to test equipment prototypes and match them to scanned 3D images showing clearances and dimensions. The software brochure indicates that interactions can be modeled to predict where surfaces would encounter compression, shear, and tension. The modeling does not appear to be part of the available package. This work apparently grew out of earlier research that used stereophotometrically recorded human body data (Beecher, 1986). Virtually all the literature that referred to stereophotometric techniques was published prior to 1990 and has been overwhelmed by the movement toward 3D digitized laser scanning techniques.

Other after-market vendors provide software that processes Cyberware output. Reverse Engineer Professional (ImageWare, Inc) was formerly known as Surfacer and is a widely used application that can be used to manipulate the point cloud produced by a variety of laser scanners for hardware or biometric applications. DataSculpt (Laser Design, Inc.) is similar to Reverse Engineer in capability. ModelGen (Software Systems, Inc.) is used for 3D visual simulation of digitized images.

An interesting set of software tools for the visualization of laser scanned images is being developed by the University of Illinois at Chicago. However, the software is being developed for internal research and is not being distributed to the public. Their LEGO visualization

software was designed and implemented to enable medical personnel to explore and manipulate laser scanned geometry obtained from a 3D laser scanner. The LEGO tools fall into three main categories: simple, quantitative, and manipulative. The simple tools allow changes to the displayed images, image processing, and labeling. The quantitative tools return measurements based on selected labeled input such as linear distances, angles, contour length and surface area. The manipulative tools smoothly deform a region by allowing selected interior points to be pushed or pulled. These tools followed the pattern of many such packages in that they are custom made for a specific narrow application (reconstructive surgery) and are not widely available (Neumann & Sadler, 1996).

2.3 Mechanical Modeling of Mask Registration - Literature Review

A major objective of the Phase I SBIR is to demonstrate the feasibility of modeling the mechanical registration of protective masks to the human face to evaluate comfort and performance of new and existing designs. To accomplish this objective, the Finite Element Method (FEM) was chosen as the simulation approach using the DYNA3D software (Whirley, 1993) as described in section 3.0. DYNA3D allows for finite deformation, nonlinear material behavior, surface contact simulation and loading functions which facilitate this modeling. The major required inputs (in addition to the geometrical model) are material models and properties for the mask, face and face/mask interface. This section presents a selective review of the literature on required material models.

The facial system (from a mechanical viewpoint) consists of bone structure with layers of different materials. The fascia, subcutaneous tissue, dermis and epidermis form the layers of interest. A significant literature base has been developed for the mechanical properties and models for the facial system. Most of this literature, however, is geared for the surgical community which is mainly interested in the membrane behavior and cutting resistance of the materials. For the mechanical registration of the mask, the most important characteristics of the system are the compressive compliance of the system (due to exerted pressure) and the shear behavior of the skin (due to frictional contact and geometrical nonuniformities. Representative examples can be found in the references.

Two approaches exist to model the facial system. The four layers described above can be modeled as a single material with properties representative of the system or modeled as individual layers with layer interaction behavior. In the surgical literature, each layer is typically modeled as a single elastomeric-like material. Finite deformation elasticity is typically chosen as the material description using a total Lagrangian formulation to account for finite deformations. While some of the literature discusses the issues of time dependent material behavior (due to creep of the tissues), this Phase I effort focused on time independent models. Various authors have reported the anisotropy in skin system response. This can have an important effect on incision choice and surgical procedure. For the mask registration problem, however, isotropy appears to be a reasonable choice.

Finite deformation elasticity requires definition of a strain energy density function in terms of the strain tensor or its invariants. For the purposes of the following discussion, it will be assumed that we will employ the Green strain tensor (represented by e_{ij}, i,j=1,2,3). Further, the symbol I_j (j=1,2,3) will stand for the invariants of the strain tensor while λ will stand for the principal stretches. J_j will stand for the strain invariants written in terms of principal stretches. A good discussion of finite deformation elasticity can be found in Green and Zerna (1968).

One form of the strain energy function proposed is described in Blatz, Chu, and Wayland (1969):

$$W = \sum_{i=1}^{3} f(L_n \lambda_i)$$

where two forms for the function f have been investigated

$$f(L_n \lambda_i) = \frac{2G}{\alpha^2}(\lambda_i^{\alpha} - 1)$$

$$f(L_n \lambda_i) = \frac{2G}{\alpha^2}\left[\exp(\alpha(\lambda_i^2 - 1)) - 1\right]$$

The undefined constants are chosen to fit the available data. An alternative function was proposed in the form described in Veronda and Westmann (1977) with a function available to fit compressibility effects:

$$W = C_1\left[\exp(\beta(J_1 - 3)) - 1\right] + C_2(J_2 - 3) + g(J_3)$$

A very complicated function has been proposed by Fung (1973) in the form:

$$W = \frac{1}{2}(\alpha_1 e_{11}^2 + \alpha_2 e_{22}^2 + \alpha_3 e_{12}^2 + 2\alpha_4 e_{11} e_{22}) +$$

$$\frac{C}{2}\exp(\beta_1 e_{11}^2 + \beta_2 e_{22}^2 + \beta_3 e_{12}^2 + 2\beta_4 e_{11} e_{22} + K_1 e_{11}^3 +$$

$$K_2 e_{22}^3 + K_4 e_{11}^2 e_{22} + K_5 e_{11} e_{22}^2)$$

which includes 13 material constants for two-dimensional problems. In Deng (1988) it is shown that many standard strain energy functions used for rubber elasticity can also be used for facial system materials.

A major problem with modeling the response of facial systems is the variability from person to person in skin thickness and elasticity, which stems from the difficulty in obtaining in-vivo data. From the data in the cited references, significant variation in the fundamental stress-

strain response exists. Some of the variation is due to in-vitro conditions which may not simulate reality while much is due to material system variability. A third factor is that the systems of interest are highly nonlinear and are very difficult to work with experimentally. Test design and execution is not possible by established testing standards. Derivation of engineering quantities (such as stress and strain) from the measurable parameters is problematic. It is not surprising, therefore, that a wide array of material models can be "fit" to the data and used for analyses. To validate any computational procedures in application, predictions must be compared with application tests to validate the entire computational procedure and not just the constitutive model.

For the analyses in this SBIR effort, we decided to limit constitutive models to the hyperelastic models in DYNA3D. The available models are the Blatz-Ko which relates the Piola-Kirchoff stress to the Green strain in the form:

$$\tau_{ij} = G\left(\frac{1}{V} e_{ij} - V^{\frac{-1}{1-2v}}\ \delta_{ij}\right)$$

A single material parameter, the shear modulus G, is required for characterization. Based on the data in the references (Crisp, 1972; Deng, 1988; Fung, 1993; Lanir & Fung, 1974; Manschott & Brakkee, 1986a; Snyder & Lee, 1975), moduli between 100 psi and 500 psi appear to span the parameter space for the available data. More complicated models in DYNA3D include the Mooney-Rivlin model which employs the strain energy function:

$$W = A\,(I_1 - 3) + B\,(I_2 - 3) + C\,(I_3^{-2} - 1) + D\,(I_3 - 1)^2$$

where A, B, C and D are constants and the Frazier-Nash model which uses the strain energy function:

$$W = A\,I_1 + B\,I_1^{\,2} + C\,I_1^{\,3} + D\,I_1^{\,4} + E\,I_2 + F\,I_2^{\,2} + G\,I_1 I_2 + H\,I_1^{\,2} I_2 + Q\,I_3 + R\,I_1 I_3$$

For the purposes of the Phase I effort, the Blatz-Ko model was employed for simplicity. For more advanced studies, however, the Mooney-Rivlin model is a good compromise between model complexity and model flexibility.

The modeling of mask registration also requires description of the mask materials. From the standpoint of deformable mechanics, the base rubber skin is the only material of interest. The remainder of the mask consists of materials which are essentially rigid compared with the rubber skin. Our literature review, therefore, focused on the rubber material.

Rubber requires a hyperelastic model as discussed for skin. The available models in DYNA3D are discussed above. Vendor data was available for representative mask rubber in the Dow Corning data sheet for TR-5 & silicone rubber. A previous analysis of mask

registration (Bitterman, 1991) was also found. Both sources indicate the modulus range for representative materials is 200 psi to 400 psi. More controlled test data with a larger number of member parameters would be required to use any model beyond the Blatz-Ko. For Phase I, therefore, the Blatz-Ko model was adopted.

The final problem of interest is the interface between the mask and skin. In the literature survey, only one study (Bitterman, 1991) has previously considered mask registration. In that study, the face was modeled as a rigid body with the mask being a hyperelastic material. The interface was modeled with rigid gap elements which creates a sort of frictionless contact problem. Since the gaps cannot conform to a complicated surface structure, some friction was numerically induced with unknown effects.

Friction between mask and face systems does not appear to have been previously studied. No references to this problem where found. It was decided, therefore, to use the friction constant as a variable in the simulations performed in this Phase I effort.

In this section, the various requirements from a material modeling standpoint were reviewed. A baseline for preliminary analyses was developed for the Phase I program. Missing data and requirements were delineated.

3.0 Finite element analysis modeling

3.1 Model Characteristics

The task of predicting the registration of a protective mask on a generic face requires a finite element analysis tool capable of modeling large deformations along a complicated sliding contact surface. One such analysis tool is DYNA3D, an explicit 3D code originally developed by Lawrence Livermore National Laboratory. This code has numerous material models and allows forces and boundary conditions to change during a simulation run.

The ability to change the boundary conditions of a run can be very useful in the case of the face and mask interaction. The mask may be constrained to move along a specified path in the process of deforming to meet the shape of the face. These constraints may then be replaced by others which allow the deformed mask to hang on the face, pulled downward by gravity, but constrained by the straps. The amount of contact between the mask and the face may then be quantified from the pressure induced on the surface elements of the face by contact with the mask elements.

The geometry of the contact surfaces of the mask was furnished as a DXF file generated by "Reverse Engineer Professional" 3D geometry application. The contact surface of the mask is a rubber material with a thickness of 0.18 inches. The total weight of the mask is 1.77 pounds. Of that total weight, the filter contributes 10.1 ounces. The modulus of elasticity for this material is not easy to obtain. A value of 400 psi is thought to be reasonable, based on characteristics of similar compounds.

The geometry of the contact surface of a generic face was furnished as a DXF file. Tissue thickness on a face varies quite a lot from point to point and from face to face. For this reason, combined skin and tissue thickness has been estimated between 5 and 10 mm. The modulus of elasticity has been assumed to be 200 psi.

Two parameters which may effect the contact between mask and the face are being investigated in this initial study. The first parameter is strap tension preload. The other parameter is skin friction between the mask and the face. Initial strap tension will be varied between 1.5 and 6 pounds per strap. The friction coefficient will be varied between 0 and 0.7.

3.2 Analysis Methodology and Validation

The process of developing a computer model of the face and mask interaction is detailed in this section. All aspects of construction are discussed from element type selection to boundary conditions. A substantial portion of the task was dedicated to learning the interaction of elements and constraints for this type of model. The first portion of the task was to determine acceptable element types for specific material types.

A large portion of the initial analysis was performed on variations of the final model to determine the interaction between various load cases and constraints. Some of this preliminary analysis is described in the analysis section.

The model is to be analyzed using DYNA3D. The selection of this code acts as a constraint on all other considerations in model development. The kinds of elements used and how they are used differ from one analysis package to another.

The initial model of the mask was composed of shell elements. This configuration proved to be stable with elastic material formulation but unstable with hyper-elastic materials. Some preliminary studies on element types were performed prior to developing a new model of the mask. The first study was performed on a 10x1 inch cantilever beam composed of either shell or solid elements with a concentrated mass at the end. The second model was that of a 1 inch cube with a 200 psi distributed load on one surface.

The cantilever beam is the simplest form of representation for the kind of motion and stresses experienced by the mask. While a positive result on the simulation may not assure a good result for the mask, a negative result will only be worsened on the mask. The cantilever beam has the added advantage of running 1000 times faster than the full mask simulation.

The cantilever beam was subjected to a gravity body force. The effective modulus of elasticity associated with bending stiffness could be determined either from the period of oscillation or from the maximum deflection. With an elastic material formulation the DYNA3D prediction provided an estimate of E closer than 1% to the input value. With a

hyper-elastic formulation the program diverged within a few hundred time increments. Shell elements could clearly not be used with a hyper-elastic material description.

The same geometry was analyzed using solid elements. Models were created with one, two and three elements through the thickness. The beam was first analyzed with an elastic material to form a base response. The one element thick beam had virtually no bending stiffness. The effective stiffness of the two element thick model was 75% of the theoretical bending stiffness. The value for the three element model was 88%.

The elastic material of the beam was replaced by a hyper-elastic Blatz/Ko model with the same effective modulus of elasticity. The word "effective" is used because the shear modulus G and not the elastic modulus E must be specified for this material. The simulation with this material provided extremely close results to the elastic material model.

This set of simulations provided the first direct confirmation that the elastic and hyper-elastic models predict the same results for small strain. They also indicate that at least three elements through the thickness are required to accurately model a shell with solid elements. This simulation also indicates that only two elements are required if bending stiffness is of secondary importance.

The solid cube is a microcosm of the interaction between the mask and the face elements. Two methods of quantifying the contact between the mask and the face were investigated. The first method for quantifying the contact pressure is the hydrostatic pressure. In using the hydrostatic stress there is an implicit assumption that shear stress plays a small role in the contact pressure. Another method is to use the principal stress component. Using this component requires the assumption that the principal stress near the surface is approximately normal to the surface. In either case, a negative value indicates compression.

A 27 element cube was loaded with a 200 psi surface load across one face. The Poisson's ratio was chosen as 0.495. The shear modulus was selected as 400 psi. The cube had dimensions of 1 inch on each side. The calculated value of either stress component should approach -200 psi as the cube oscillations damp out to steady state. Figure 2 shows a typical deformation of the cube during the loading where two of the faces are constrained. This model simulates the case of infinite skin friction between two contact surfaces. The darkened element is the one being followed for the time history. Figure 3 shows the typical deformation of the cube when one of the faces is unconstrained. This model simulates the case of zero skin friction between two contact surfaces. As with the constrained case, the darkened element is the one being followed with the time history. The reason for following a side surface element rather than the center element is to determine if shear stress substantially effects the results.

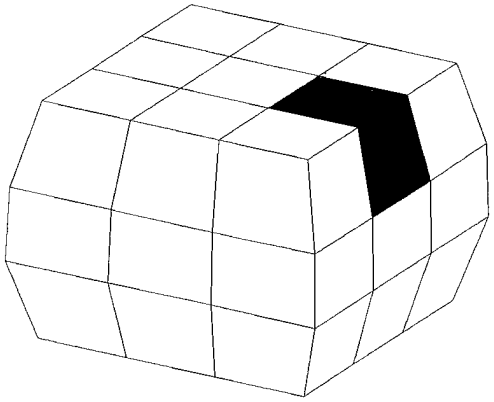

Figure 2. Deformation of 27 Element Cube With No-Slip Surface

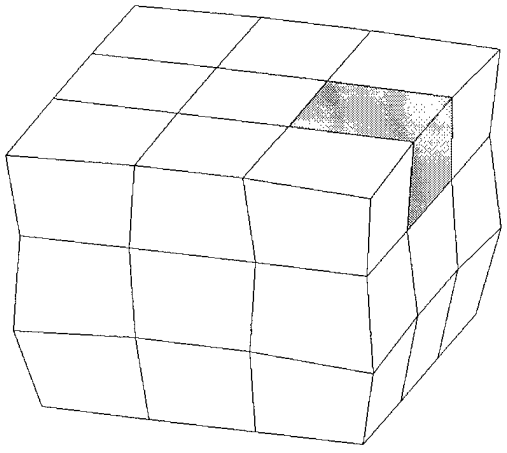

Figure 3. Deformation of 27 Element Cube With No Skin Friction

Figure 4 shows the stress prediction for the two simulations. The quantity smax in the legend box refers to the principal stress. The quantity 's hyd' refers to the hydrostatic stress. The correct value for contact stress is -200 psi. The value predicted by the hydrostatic stress is about 60 psi, for zero skin friction, and 80 psi for infinite skin friction. This value is clearly too low to be an adequate measure of the contact stress. The principal stress by contrast provides a fairly close estimate of the actual surface pressure independent of the shear stress.

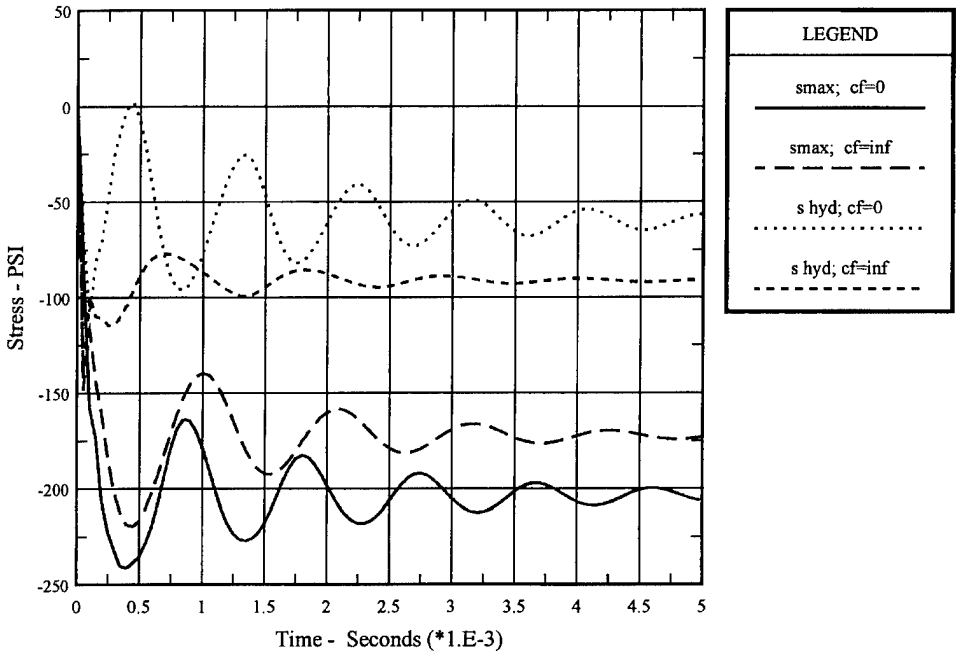

Figure 4. Stress History Comparisons For Surface Element

Although not shown, this analysis was performed with Mooney-Rivlin hyperelastic material as well as the elastic material model. The simulations all fall on top of each other. This is because these compressive loads are effectively small strain response. The materials begin to act differently with large strain, where elongation may be 500 to 700%.

The effect of Poisson's ratio on the stress history was also investigated. In a typical engineering analysis the value of the Poisson's ratio is simply set to 0.3. A 5% change in this value will not significantly alter the results. For hyper-elastic materials a 5% change could make the material completely incompressible. The Poisson's ratio for these materials is somewhere between 0.47 and 0.50. Figure 5 shows the effect of the Poisson's ratio on the time history of the principal stress for the zero skin friction case. Notice that the primary

effect of increasing this ratio is to add viscous damping into the solution. Increasing the Poisson's ratio also slightly increases the material stiffness but this is clearly a small effect.

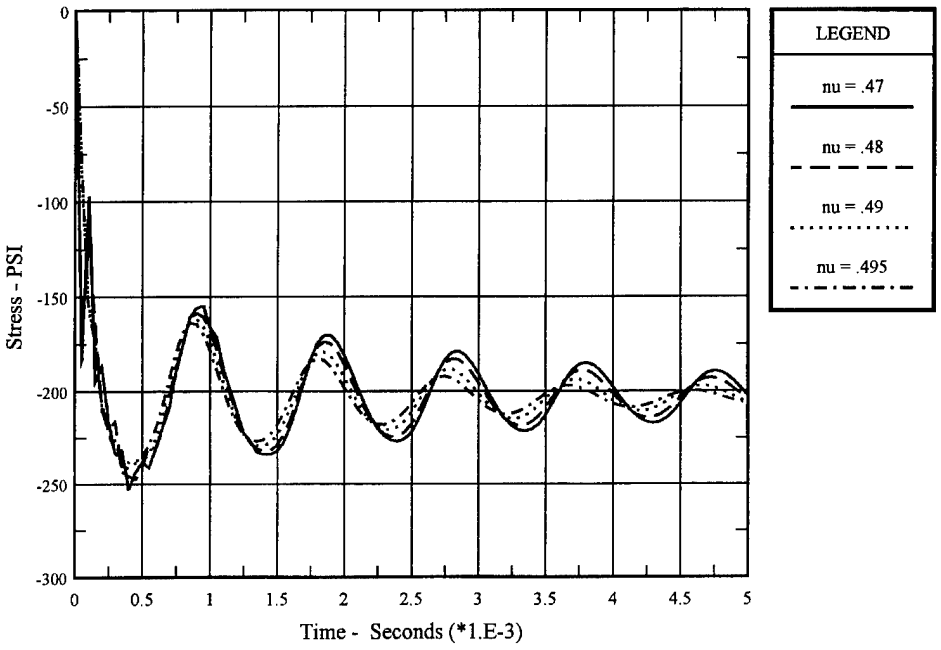

Figure 5. Effect of Poisson's Ratio on Stress History

The primary components of this model were the face and mask elements. The two components are shown together in Figure 6. Only solid elements were used to model both the face and the mask for this task. Shell elements were generated as an intermediate step in the creation of the model but were not used as part of the structure. Shell elements also provide a way of tracking nodes on the surface of a solid and the connectivity of these surface nodes. That is, the shell elements generated as an intermediate step also define the sliding surfaces.

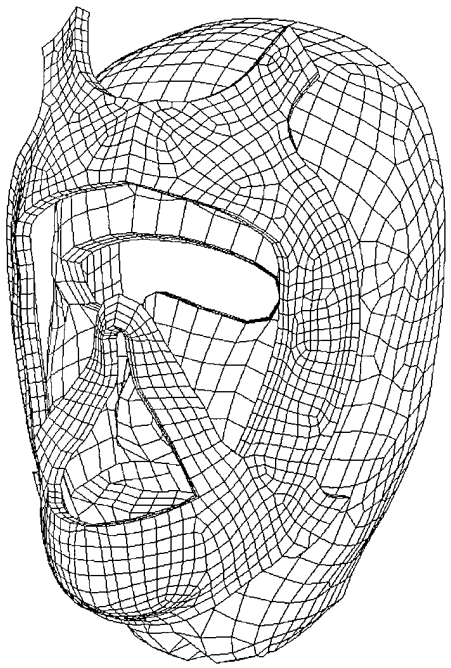

Figure 6. Initial Geometry of the Face and Mask

Considering that the mask undergoes large displacements but relatively small strain, either the Mooney-Rivlin model or Blatz-Ko model may be used. The Blatz-Ko model is inherently simpler than the Mooney-Rivlin model. Only two inputs are required to specify this model; the shear modulus and the Poisson's ratio. A Poisson's ratio of 0.48 was used for both the skin and mask material models. A shear modulus of 67 psi was used for the skin. For the mask a shear modulus of 134 was used. This corresponds to tensile moduli of 198 psi and 397 psi, respectively. Shear modulus, G, is related to tensile modulus, E, and Poisson's ratio, p, via the formula:

$$G = E/ [\ 2*(1+p)\ ] \quad p = 0.48$$

The face was modeled in several steps. In the first step, the lines of the DXF file were used to create temporary nodes on the face. The original data included only the primary contact area of the face. Through initial simulations, it was determined that the registration contact zone was larger than the geometry available from the scan. This is due to the distortion of the face and mask surfaces during the registration process. In order to assure that no gaps occurred in the contact, the contours of the face were extended through extrapolation. The contours of the face were extended by extrapolating the existing data onto a plane 5 inches back from the existing data and then fitting smoothed lines between these points. An outer

surface of the face was generated from a combination of lines fitted through the data. This outer surface was meshed to create shell elements in place of the surfaces.

This shell element representation of the face was copied to another layer and reduced in size by approximately 5%. This new set of elements then formed the inner surface of the face. The inner and outer surfaces were separated by about 0.25 inches. The solid element representation of the face was created by generating elements between the two shell element entities. This solid representation of the face was three elements thick. A three element thickness is the minimum number required to provide a ± 10% accuracy in the solution.

The nodes associated with the inner surface of the face were constrained in all six degrees of freedom. The elements of the outer surface were later used to determine the connectivity of the master surface.

The mask was created using a DXF file as a template for the geometry. As with the face, a surface representation of the mask was first generated, followed by a shell element representation. The solid elements were generated by extruding the shell elements in the direction of their normals a distance of 0.18 inches. The resulting solid body was two elements thick. A two element thick body will have accurate tension response but will have about 25% error in the bending response. This level of error is acceptable for the bending stiffness in the mask because an accurate stress profile in the mask is not required to get a representative stress distribution on the face.

The shell elements used to generate the mask and the shell elements used to generate the face were well suited to define the sliding contact surfaces associated with the interaction between the face and the mask. The shell elements associated with the outer surface of the face were selected as the master elements. The orientation of these elements was such that the surface normals pointed out of the face.

The shell elements associated with the mask were selected as the slave elements. The surface normals of these elements pointed into the face. The normals of the two contact surfaces thus pointed at each other.

The total weight of the mask is 1.77 pounds. The rubber material of the mask has a density equivalent to water. The calculated volume of the mask is 7.019 cubic inches. The weight of this material is therefore 0.244 pounds. The filter has a known weight of 10.1 ounces or 0.631 pounds. This leaves 0.895 pounds unaccounted for by the model. This 0.895 pounds was considered as non-structural mass and was evenly distributed on the nodes associated with the inner border of the mask, excluding the nose piece.

The basic components of the model were defined in the previous section. The constraints for the interaction of these components is discussed in this section.

The mask is first moved onto the face by pulling the straps. To prevent the mask from being pulled away from the desired contact point, a constraint to the motion is applied. In the first

step, new node points are defined at the same locations as the distributed masses. These nodes are constrained to move as group with the same displacements and only in the y direction. Discrete springs are defined between these new node points and the node points associated with the distributed mass. The mask can therefore flex about these distributed mass points. The amount of flexure can be controlled using a spring constant. The spring constant is set to 2.0 lb/in. to allow the mask to flex but not translate. In addition, viscous damping is created between the same nodes with a magnitude of 1.0 lb/(in/sec) . The modeling used in this effort fully allowed for sliding and stretching of the mask.

The face is prevented from moving by constraining the inner surface of the face, described in section 3.2. These shell element definitions are first used to generate the solid elements and then to define the constrained nodes. Once these constraints are defined, the shell elements may be removed.

There are two distinct body loads applied to the model. The first load is a lateral acceleration in the y direction. This load is used to move the mask as a unit towards the face. The second load is vertical acceleration applied once the mask was in contact with the face. This load simulates the weight of the mask on the face. Figure 7 shows the acceleration profiles used in the final runs of the model. Notice that the two loads are applied at different times. The load in the y direction is applied to start the simulation. The load in the z direction is applied once the model has contacted the face and is constant thereafter.

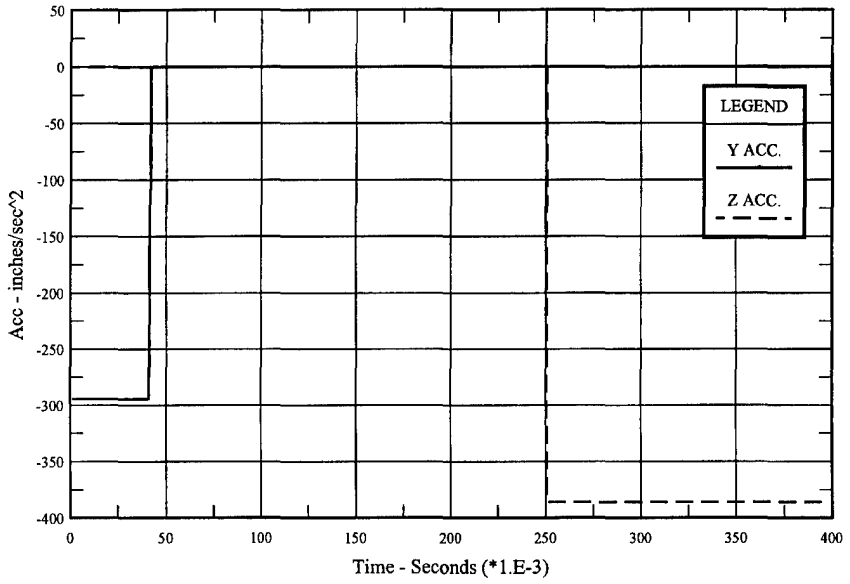

Figure 7. Body Loads Applied to Face and Mask Elements

There are a total of six straps to hold the mask on the face. In the geometry model available from the laser scans, only four straps were included. For this Phase I feasibility study, only four straps were modeled (no cheek bone straps were included). Strap loads are applied at the nodes associated with the ends of the straps. A force multiplier may also be specified for the strap loads so that strap loads may vary as a function of time.

There are 15 nodes associated with the ends of each of the top two straps in the current model. As Figure 6 shows, these straps pull along the top of the forehead and away from each other. Each node is given a force of -0.05 pounds in the y direction and 0.025 pounds in the x direction, away from the y axis. For a multiplier of 1.0, the total force per strap would be (0.375 , 0.75, 0.0) pounds.

There are also 12 nodes associated with the straps above the cheek bones. The force per node is set to the same value as for the upper straps. For a multiplier of 1.0, the total load per strap is then (0.3, 0.6, 0.0) pounds.

There are 18 nodes associated with the ends of the lower straps. During qualitative observations of three mask users it was noted that the strap force due to this strap was lower than that of the upper strap. For this reason the force per node is set to 0.035 pounds. The node force in the x direction is set to 0.018 pounds. The total force per strap is then (0.324, 0.63, 0.0) pounds. The sum of the forces due to the six straps is thus 3.96 pounds, with a force multiplier of 1.0.

As an alternative to setting a nodal force on the ends of the straps, a prescribed velocity profile was tried for the strap ends. This velocity profile was calculated to provide a certain amount of stretch in the straps after the mask made full contact with the face. This option will be described more fully in the next section.

3.3 Simulations

All of the parameters required to perform the analysis have been detailed at this point. There is a certain learning curve associated with applying all of these parameters to a simulation in a manner which gives meaningful results. The following section discusses some of the steps required to get to the final analysis model.

The advantage of prescribing the velocity of the strap end points is that the problem may be run without changing the boundary conditions. The problem is that the end point for the node travel must be known before the problem is run. Small changes in this selected end point can make the mask much too loose or much too tight. After a few tries this loading profile was abandoned.

Strap loads were defined for this model without otherwise constraining the motion of the mask. This load type was abandoned after just a few tries. The mask would slide off of the

face without precisely balanced strap loads. Even when the loads were balanced, the rest point would change dramatically with skin friction coefficient.

After the problems with the first two load conditions the problem was split into two parts. In the first part, the mask would be moved to a specific location with a specified load. In the second part, the ends of the straps would be fixed and the mask allowed to shift as required. To perform the second part of the problem required that the boundary conditions be changed and the problem restarted.

The strap loads defined in section 3.2 were used in conjunction with the spring loads also discussed in that section. These strap loads were applied gradually and then maintained at a constant level. Figure 8 shows the load factor as a function of time.

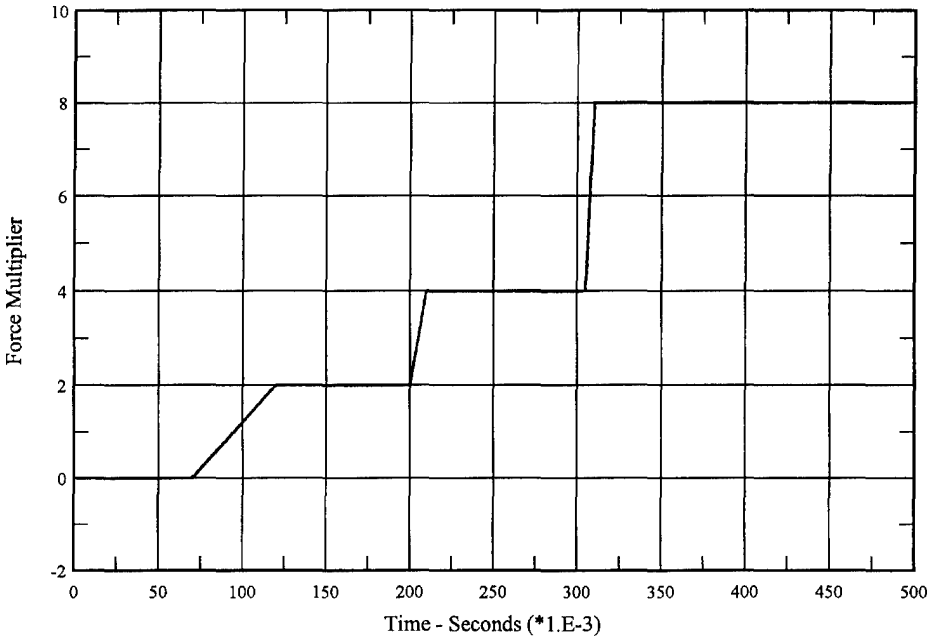

Figure 8. Strap Load Factor Time History

The problem was run for 400 ms so that quasi- static conditions were obtained on the mask. Figure 9 shows a representative deformation of the mask on the face after one such run. At his point the mask position is still constrained and the body load in the z direction has not yet been applied. The mask is seen to slide around the surface of the face and conform to the outer contours of the face rather than penetrate the surface of the face.

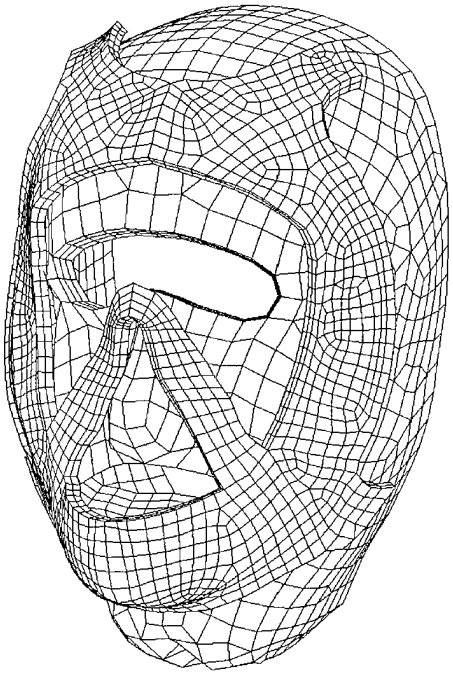

Figure 9. Deformed Shape of Mask on Face

In the next step of the simulation the positions of the end points of the straps are constrained to the locations reached at the end of the strap force constrained simulation. All other motion constraints on the mask are relaxed and the body of the mask allowed to sag under the force of gravity. The simulation is run 300 ms with these constraints in place.

The initial shape of the face created extremely high pressures, at the temples and cheek bones, when full contact was achieved between the mask and the face. This force could be reduced with a thinner face or softer material for the face. The width of the face was reduced to 92.5% of the original width. Reducing this width cut the maximum stresses by about 30% on the cheeks compared to the original geometry.

The final settings for this simulation were determined from these preliminary runs. the settings are detailed below.

Body Loads	The body loads described in section 3.2 were used to initialize the motion of the mask and then provide a steady gravity load.

Strap Loads — The strap loads described in section 3.2 were used to load the mask during the initial 300 ms. of the simulation. Load factors of 2, 4 and 8 were applied to this mask. The total force pulling the mask toward the face is approximately 8, 16 and 32 pounds with these load factors.

Skin Friction — Three different skin friction coefficients were used in the simulation of interaction between the mask and the face. These values were 0.0, 0.1 and 0.7. The value of 0.1 is assumed to be the most likely value. This assertion is based on friction constants between dissimilar elastomers.

During the first 400 ms. the motion of the mask is constrained to the y direction by the spring/damper system described in 3.2. The body loads and a strap load profile from 3.2 were used. The skin friction coefficient was either 0,0.1, or 0.7. A restart file is generated every 100 ms.

The simulation is restarted at either 200, 300 or 400 ms with the reset constraints of 3.3. The simulation is run for another 300 ms. The restart times are associated with strap total loads of 8, 16 and 32 pounds.

There were a total of 5 cases run as part of the actual analysis. The 5 cases are described below.

Case 1 represents the nominal definition of mask and face parameters. It was restarted at three different times to get the effect of different preloads, from 8 to 32 pounds. The skin friction coefficient was set to 0.1 for the sliding contact surfaces.

Case 1a. The simulation was restarted at 200 ms. to mimic the effect of an eight pound preload on the straps and run for an additional 300 ms. The actual load on the straps changes as the mask settles.

Case 1b. The simulation was restarted from 300 ms. to mimic the effect of a sixteen pound preload on the straps and then run for an additional 300 ms.

Case 1c. The simulation was restarted from 400 ms. to mimic the effect of a thirty two pound preload on the straps and then run for an additional 300 ms.

Case 2. The skin friction coefficient was set to 0.0 and the simulation run for 300 ms. to mimic the effect of a sixteen pound preload. The program was restarted with fixed strap positions and run for an additional 300 ms.

Case 3. The skin friction coefficient was set to 0.7 and the simulation run for 300 ms. to mimic the effect of a sixteen pound preload. The program was restarted with fixed strap positions and run for an additional 300 ms.

Case 1 was run to show the effect of strap load on contact pressures and total surface contact. Case 2 and 3 were run to get the effect of skin friction at a constant strap load.

3.4 Results

An experimental study of the surface contact pressures was performed by HRED (Cohen, 1996) and was used during this effort as a means of validating the simulation. In this experiment, contact pressures were measured at thirty degree intervals around the face. The precise locations have not been provided so approximate locations were found on the model of the face. There were 11 locations on the face where pressures were measured. Figure 10 shows the locations on the model for each of the stations. Notice that stations 1, 6 and 11 have two elements rather than just a single element. For these stations, the element pressures are averaged. This was done to smooth the element response between different load cases.

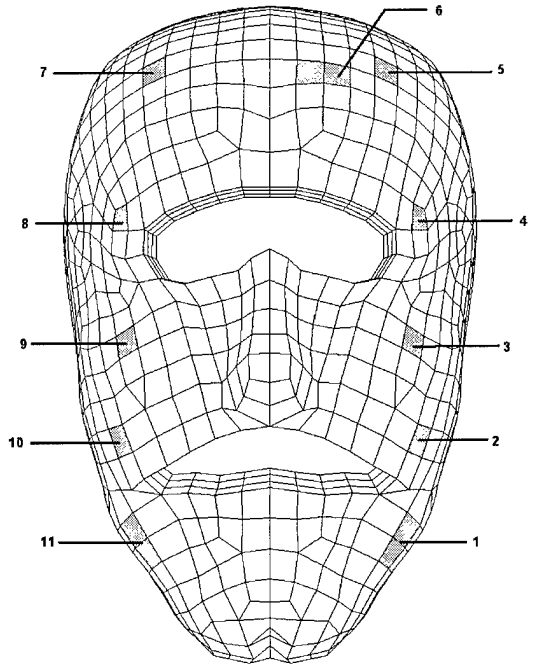

Figure 10. Stations for Surface Pressure Sampling

The contact pressure at various stations around the face is shown in Figure11. The principal stress was calculated in PSI during the analysis. After the analysis the stress values were

multiplied by -70.3 to convert a compressive stress in PSI to a positive pressure in grams per square centimeter. There are two curves for the experiment which show the extremes of the pressure data. One curve represents the maximum for all tests and one curve represents the minimum for all tests. There are also two curves for the simulation of the mask and face interaction. The low curve represents Case 1a, an eight pound preload. The higher curve represents Case 1b, a sixteen pound preload. The pressures for Case 1a are generally less than the minimum values of the experiment. The pressures for Case 1b are generally larger than the experimental results. The trends are also in agreement between prediction and experiment. This indicates that good agreement between simulation and experiment should be obtained with a twelve pound preload, or about two pounds per strap.

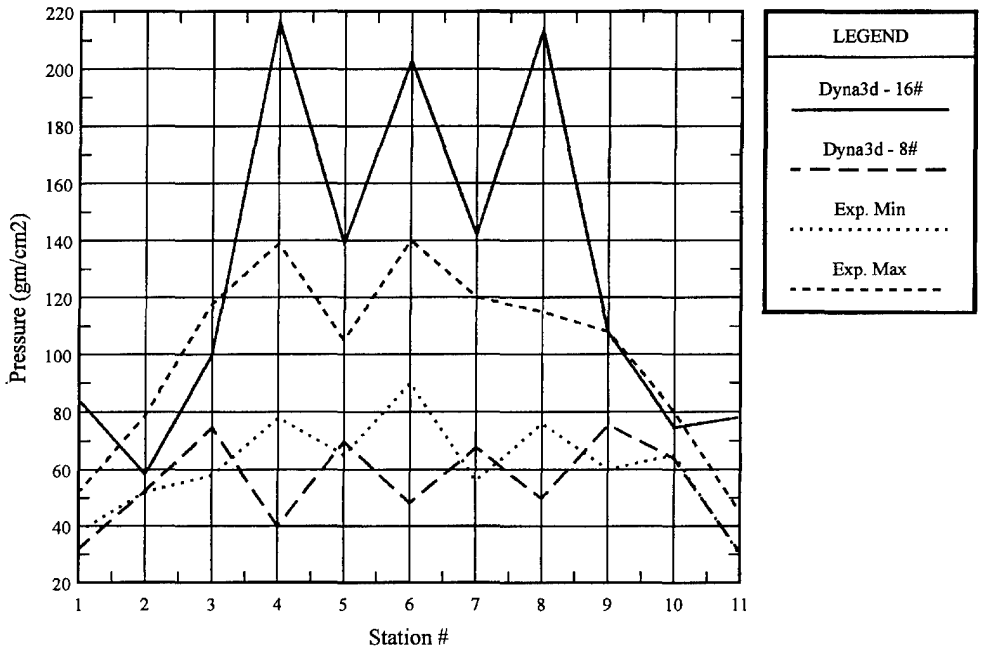

Figure 11. Surface Pressure Comparison Between Simulation and Experiment

The agreement between the model and experiment indicates that the two share some common features. Pressure peaks found in the prediction should indicate high contact areas for the actual mask. Figures 12 and 13 show the principal stresses in PSI on the surface elements of the face.

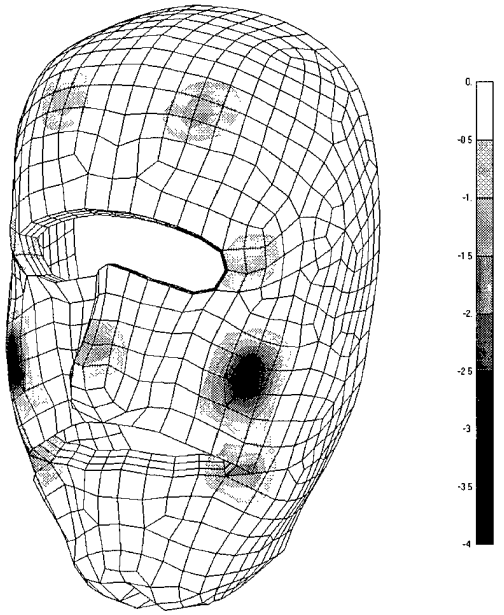

Figure 12. Principal Stress on Face With F=8 and Cf=1

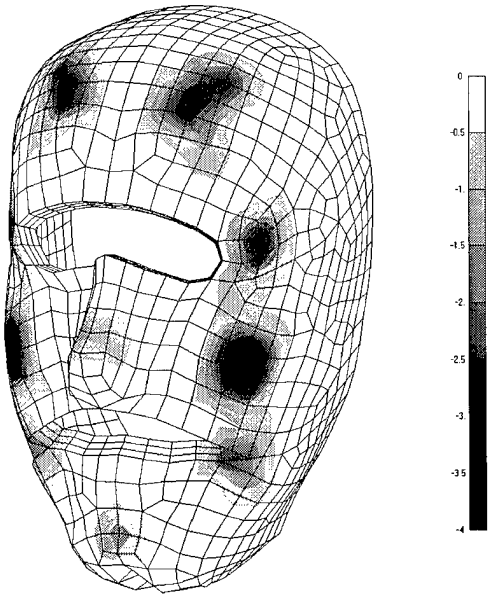

Figure 13. Principal Stress on Face With F=16 and Cf=1

It should be noted here that the principal stress contour plots are not truly accurate. They are generated by first creating node values using the average values of all coincident elements. Contours are then generated by interpolating between nodal values. Areas with steep gradients are thus smoothed out over several elements. These contour plots provide distinctive visual information but not precise element values.

For Case 1a Figure 12 shows that the chin has no forces on it and one portion of the cheek has a high stress. The bridge of the nose has a small load due to contact with the nose piece of the mask. This figure shows that the contact with the cheek is preventing full contact with the rest of the face.

From Case 1b Figure 13 shows that doubling the load allows full contact between the face and mask. The stress on the nose is unchanged. The stresses on the forehead, temple and cheeks have increased proportionally to the load. The load due to the lower strap is almost unchanged. Instead, this added strap load is being applied to the chin.

Figure 14 shows the contact pressure associated with Case 1c, a 32 pound preload. This figure shows that the mask has fully deformed to fit the contours of the face. The pressure distribution is seen to be above 1 PSI around the contours of the mask.

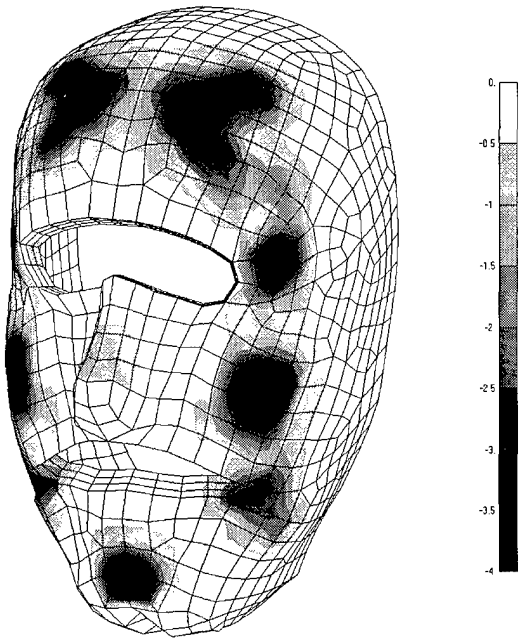

Figure 14. Principal Stress on Face With F=32 and Cf=1

These three figures show the outline of the forehead straps through the pressure profile. The nose piece does not provide a substantial load to the bridge of the nose. The cheeks are seen to be creating an obstruction to a proper seating of the mask.

The effect of skin friction on the pressure profile is demonstrated by Cases 2 and 3, shown in Figures 15 and 16. With skin friction reduced to 0 the mask is more free to slide during the strap preload portion of the simulation. Once the run has restarted the strap positions are fixed and the effect is similar to a higher load. The stresses for no skin friction are thus seen to be higher than those for a skin friction coefficient of 0.1. By comparison, the stresses for a large skin friction coefficient are smaller. The lack of coloration at the chin indicates that the bottom of the mask has not made contact with the face.

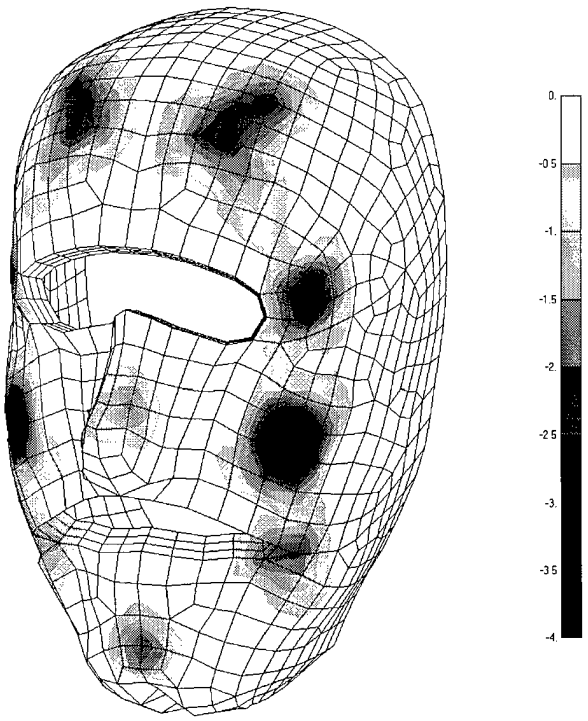

Figure 15. Principal Stress on Face With F=16 and Cf=0.0

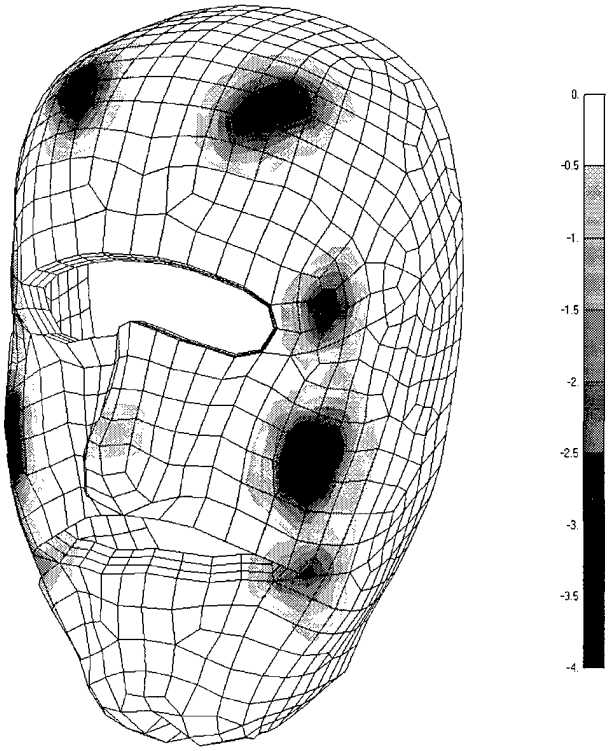

Figure 16. Principal Stress on Face With F=16 and Cf=0.7

There are substantial differences between stresses in Figures 15 and 16. The reasons for these differences cannot, unfortunately, be attributed to a single parameter. The effect of skin friction during mask settling is being overshadowed by the effect of skin friction during the preload. To see this effect, note that the stresses obtained after settling are defined by constraints of both skin friction and strap endpoint position. The strap endpoint is, however, significantly altered by skin friction during the preload. The effect of skin friction is therefore a combined effect in the current model and not separable item, as it should be.

4.0 3D laser scanning

As part of the Phase I effort, DCS investigated the feasibility of using laser scanning technology as a means of providing the surface image of the physical bodies that must be modeled to perform the analyses regarding fit and discomfort. DCS used our in-house 3D Areal mapper as the instrument to perform the laser scanning of the M40 mask and a face. A 3D scan of the M40 mask face seal and nosecup was the item of primary interest. The file from this scan was converted to DXF format and was modified to form a series of surfaces

that could be used by the FEA software. Since the FEA software used in this Phase I feasibility study had an upper limit on file size, and the analysis was limited in scope, the resolution of the scan was adjusted so that the computational burden was manageable. In addition, the same system was used to produce an image of a representative face. To check the quality of the data, the files were displayed as 3D images on a Silicon Graphics Indigo 2 workstation. The images were rotated and viewed from various perspectives to check the quality of the images. The face model and seal model were exported to the FEA software so that the FEA analysis could proceed. The FEA analysis has successfully been performed using the input files of the mask seal and face from the laser scanner as discussed in section 3.0.

The 3-D Areal Surface Mapping System

DCS has developed an improved topographical mapping system, the 3-D Areal Mapping System,. This system operates by projecting a structured multiple-line laser light array onto a target surface, temporally modulating the array, sensing the reflected light with one or more off-axis video cameras, and triangulating along the center of each line in the array. The structured laser light array, is generated using an interferometric technique from a single laser beam. DCS has patented a novel holographic element for generating this array with a minimum of optical elements.

To make possible the unique identification of each line as observed on the target's surface, the laser projector passes the structured laser array through a liquid-crystal Spatial Light Modulator (SLM). The SLM allows the host computer to turn on or off any line or combination of lines. Obviously, the system could function by projecting one line at a time. With one exposure per line, this would take N video frames to uniquely identify N laser lines. The Areal Mapper reduces this to $\log_2 N$ by projecting a binary sequence of patterns onto the surface of the target: one image with all lines on, one with the first half on and the second half off, one with quarter on/quarter off/quarter on/quarter off, and so forth. By correlating a complete series of such images, with the target held stationary during the sequence, the computer can determine which row in the structured light array a particular line, as observed on the surface of the target, is associated with and then solve the equations to locate any spot on the target's surface, located on that line, in 3-D space. The SLM used is capable of switching patterns during the vertical retrace time of the video camera, so patterns may be acquired in successive video frames. Given a laser array with 128 lines and a standard 30 frame/sec camera, 8 frames ($\log_2 128$ + one image with all lines turned off) are required, for a total acquisition time of 8/30 seconds. This time could be reduced further if high-speed digital cameras, such as those produced by Q-Dot of Colorado, were used, although such cameras are significantly more expensive than conventional cameras.

For the field of view covered by the laser projector and camera at one point in time, no mechanical movement of either the target, the laser projector, or the camera is necessary. All components of the laser projector and the camera are electro-optical and non-moving; thus once the system is calibrated it will retain its accuracy. In addition, the system handles non-optimal surfaces well. Since, during processing, the system effectively has images of the area

illuminated by each stripe both with the stripe turned on and with it turned off, but with no other changes to the image, it can readily determine the extent of the laser line even under wide variations in target surface reflectivity.

One important feature of the structured laser light array used in the Areal Mapping System is that it does not have a focal point. The array diverges as it propagates from the laser projector, but the stripes are always a fixed proportion of the size of the overall array, and are always sharp and well defined. This, in turn, means that the array may be expanded or contracted to cover any desired field-of-view by moving the target or the projector. Additionally, the divergence of the beam may be controlled optically through lenses so that it is a desired size at any distance from the projector and/or diverges/converges at any desired rate. The lower limit on the size of the array is limited only by the diffraction limit of the optics used; DCS has calculated that a line spacing of less than 10 microns is easily attainable. The upper limit is set only by the room available for divergence, the laser power available, and the sensitivity of the cameras used (enough light must reflect from the target surface along each line to satisfy the camera's signal-to-noise requirements). Projector to target distances of many tens of meters and array dimensions of several meters are feasible.

The resolution and accuracy of the Areal Mapper are determined by the number of laser lines projected and by the resolution of the CCD camera. For a 1 inch square field-of-view (FOV), given a 256 line projector (as DCS projects for a first-generation production unit) and a 624 pixel x 480 line CCD camera (a standard size), the system will have a line-to-line spacing - and an over all system resolution - of 1/256 inch, or about 4 mils. The overall system accuracy is determined by the resolution of the camera and would be +/1 one pixel, or 1/624 inch (about 2 mils).

Accuracy, resolution, and overall mapping speed are directly proportional to the size of the FOV. Generally, the system's field-of-view is set to achieve the desired minimum accuracy. Then, if the FOV does not cover the entire desired target area, either the target or the system is moved to tile together adjacent views. This issue is addressed in more detail below.

The Areal Mapping System yields one additional capability: since conventional cameras are used, gray-scale (or, optionally, color) images of the target are also available. These may be used for visual inspection or for additional automatic image processing.

DCS Proof-of-concept Prototype System

Two years ago, DCS applied for a grant from the Department of Energy/National Institute of Standards and Technology (DOE/NIST) Energy Related Inventions Program (ERIP). This program grants funds to small companies in an effort to bring to market technologies that result in energy saving or conservation. In its application, DCS proposed a variation of the Areal Mapper optimized for the inspection of turbine blades in high-pressure steam turbines and jet engines.

In October, 1994, DCS was awarded an ERIP grant and commenced development of a demonstration prototype inspection system. Intended as a demonstrator for potential customers, the prototype is optimized for the inspection of turbine and compressor blades, and will demonstrate the increased speed and accuracy possible with the DCS approach. The prototype uses primarily off-the-shelf components, with the exception of a DCS-developed holographic optical element, including a DisplayTech Inc. (Boulder, CO) 64-line SLM. Video images of the pattern, as projected onto the target's surface, are captured by a CCD video camera and digitized by an image processing board in the host computer (a Pentium-based PC).

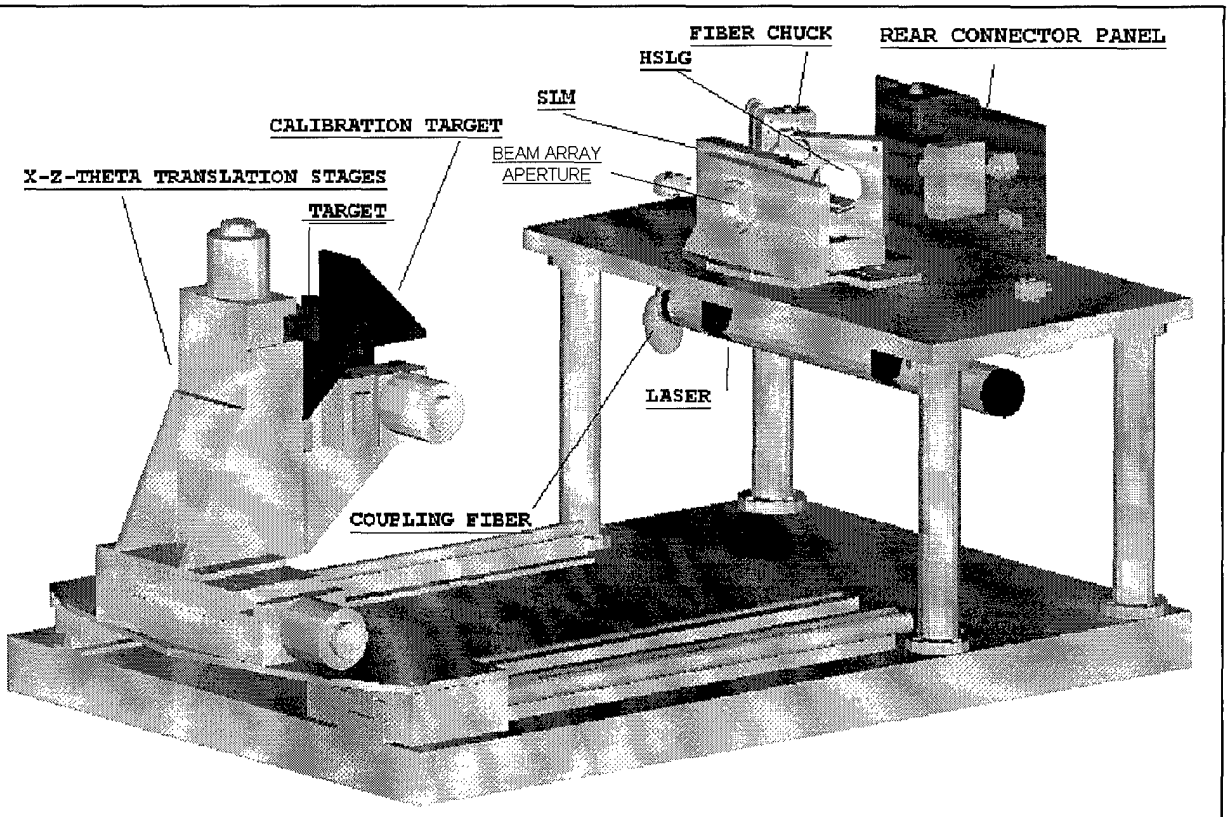

Figure 17. 3-D Areal Mapping System Prototype, Rendering

The prototype is shown in a CAD rendering in figure 17; the laser projector is on the platform on the right, the target goes on the 3 axis positioning stage at left (the video camera is not shown but it is located on a separate platform above the laser projector). The laser array diverges from the laser projector at approximately 12 degrees. By moving the stage on the rails (towards/away from the projector) the size of the array on the target may be varied from less than one inch high to almost 6 inches.

This system can capture one field of view, with up to 20,000 3-D data points, in less than one second. Even though processing power is limited, the captured images can be processed into a

map file in approximately one minute, for a total data throughput of approximately 700 points per second. With a 2" x 1" field of view, a typical setting, the system resolution is on the order of 30 mils vertical (distance between stripe centers) 5 mils horizontal, with overall system accuracy on the order of +/- 10 mils. The accuracy is limited at present by several factors, especially the machining accuracy on the calibration target and the limited error correction and filtering done in the mapping calculations.

Application of the 3-D Areal Mapping System Prototype to Respirator/Human Face Interface SBIR

DCS used the prototype 3-D Areal Mapping System to map a respirator and a human face in support of the Respirator/Human Face Interface SBIR effort. The sealing surfaces of the respirator were mapped in order to characterize it for CAD representation and use in the finite element analysis. The face of a DCS employee was mapped in two expressions, with otherwise identical location, in order to get representative anthropometric data.

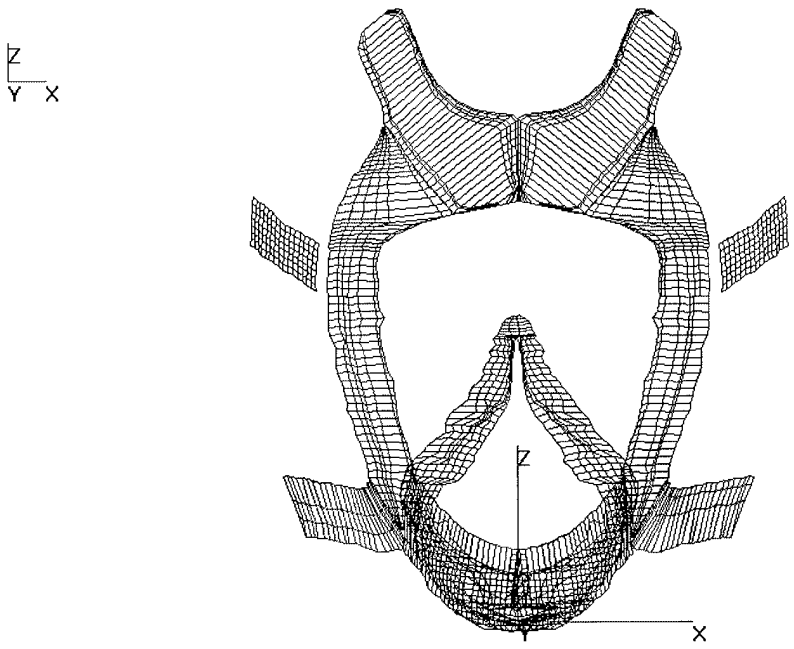

Figure 18. Protective Mask Seal Map Representation

Figure 18 shows the seal area of the protective mask, after surfaces were fitted to the acquired data points, using the ImageWare, Inc. *Reverse Engineer Professional* program. *Reverse Engineer Professional* is a commercially available program for processing the output from 3-D digitizers and scanners, and is used to convert the raw point clouds generated by the 3-D Areal Mapping System into surfaces that can be manipulated by AutoCAD. The surfaces shown in figure 18 were exported into a DXF format file and processed to form a CAD representation of the mask.

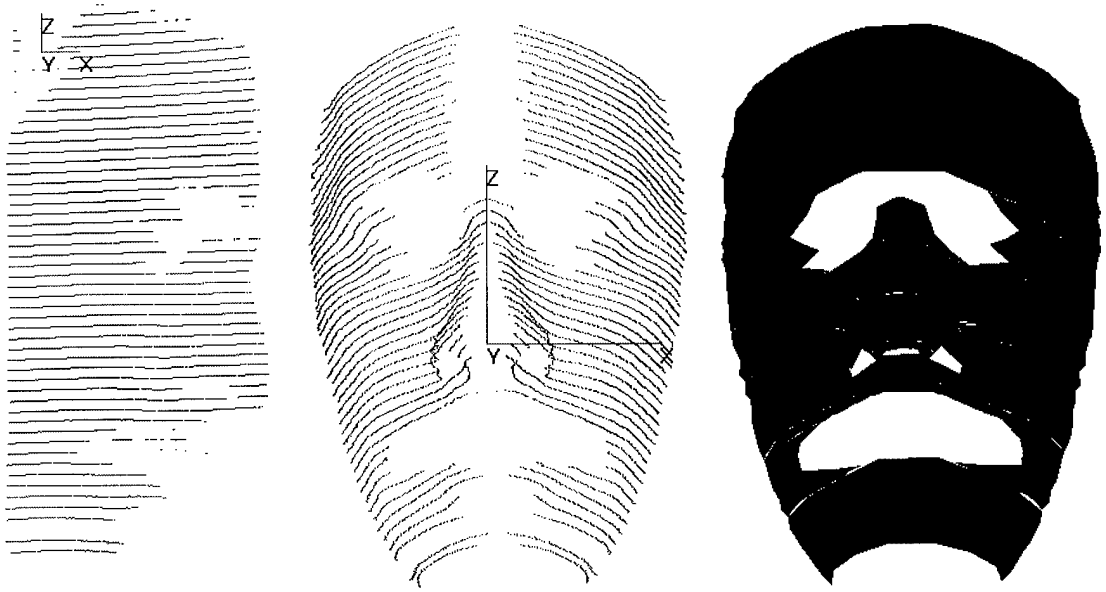

Figure 19. Face Map, Expression 1

Figure 20. Face Map, Expression 2

Figure 19 and figure 20 show maps of a human face in two different expressions. In each case, the face was mapped from one side only and the map reflected during processing with *Reverse Engineering Professional* to obtain an entire face. From left to right, the figures show the

original point cloud, from the side; a frontal view of the full point cloud set, consisting of the original 1/2 face set and its mirror image; and the surface that was fit to the full point cloud set. There were problems with data collection around the mouth and eyes, due to facial hair and the use of only one camera angle, but the important areas of the face that contact the protective mask seal were adequately imaged.

The main problem with the use of the prototype DCS 3-D Areal Mapping System for this effort was that, as described above, the prototype was designed for the mapping of small objects such as turbine blades. For an object the size and complexity of the protective mask, the prototype does not have adequate translation or rotation capability. Remembering that in order to map a complex object, smaller fields of view are mapped and tiled together; the positioning system needs to be able to present each surface to be mapped to the laser projector and video camera. Specifically, the prototype has only one rotational axis, 6 inches of travel in X and Y, and no motorized capability in Z. In order to properly digitize the mask, 8 inches of travel in X, Y, and Z would have been required, with at least 2 orthogonal rotational axis.

For an object like the human face, where it is obviously impractical to fasten the subject to a turntable and hold him still during the mapping process, a preferable system would have had multiple projectors and cameras in a circular configuration around the head, mapping in close sequence. Also, in order to capture the 3-dimensional shape of the face as the subject contorts it, as when reading the "rainbow passage" test phrase, a system that can acquire maps at a rate of around 30 maps per second is desirable. For this project, the available prototype could only acquire from a single point of view, at a rate of approximately one map per second. A high performance system capable of faster data collection rates is in the planning stages, but is not yet available.

5.0 AutoCAD Modeling

During this effort the primary use of the scanned images was to form a model of the M40 mask sealing surface around the periphery of the mask and the nose cup which was then used in the FEA analysis. A second use of the 3D scanned images was to generate a CAD model of the M40 mask using AutoCAD software. For this application, the raw point cloud generated by the laser scanner was used by the AutoCAD operator. Starting from this point cloud he was able to link the points and create a representation of the mask. The CAD model of the external surfaces of the M40 mask is shown in figure 21 below. This figure shows an AutoCAD model of the M40 using extruded polyline triangular facets. The model was generated using imported images from the laser scan of the mask peripheral seal, data from drawings of the mask, and physical measurements of the actual mask when dimensions from the drawings needed to be verified or reconciled. Figure 22 shows a rendering of the same mask model using the rendering capability resident in the AutoCAD application. The purpose of this model was to provide the basis for the analyses required to address fit and discomfort. No attempt was made to model mask details such as lenses, voicemitters, valves, etc. that did not play a direct role in this analysis. These bodies were modeled as solids with the appropriate characteristics. The AutoCAD model of the M40 molded rubber body is

annotated with the material properties that were generated as a result of the literature search in section 2.3 and the analyses in section 3.0.

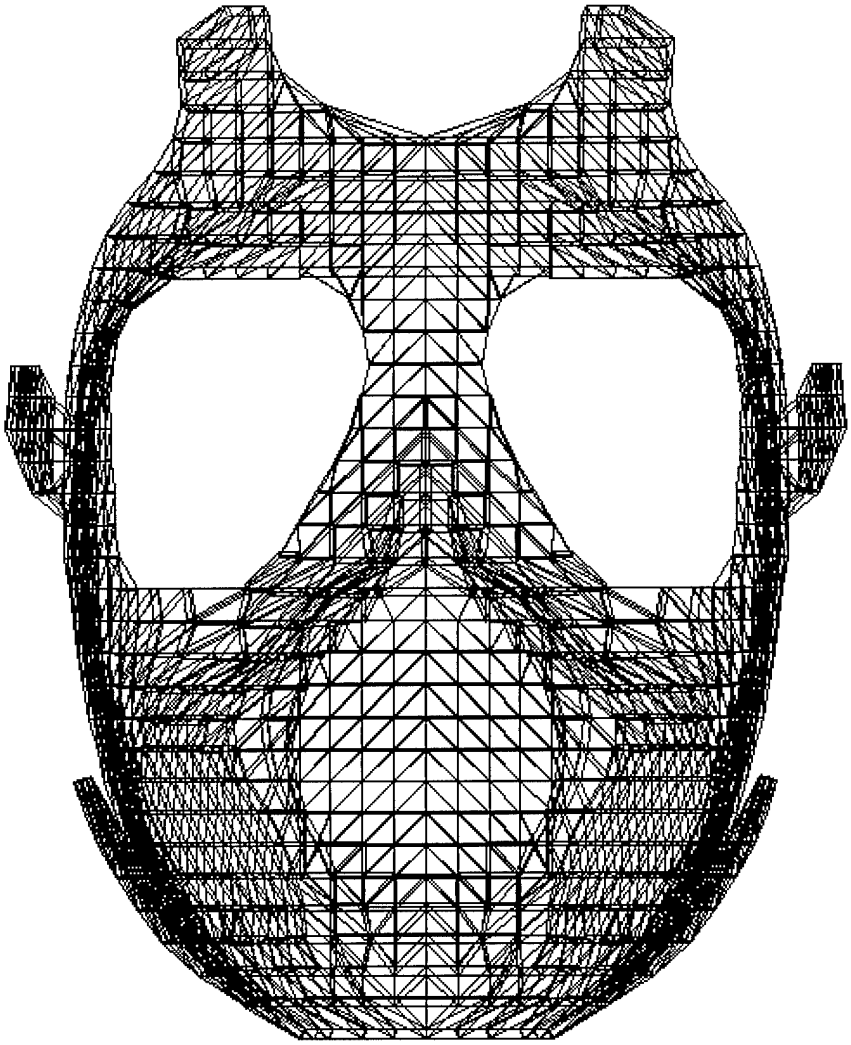

Figure 21. M40 mask AutoCAD model

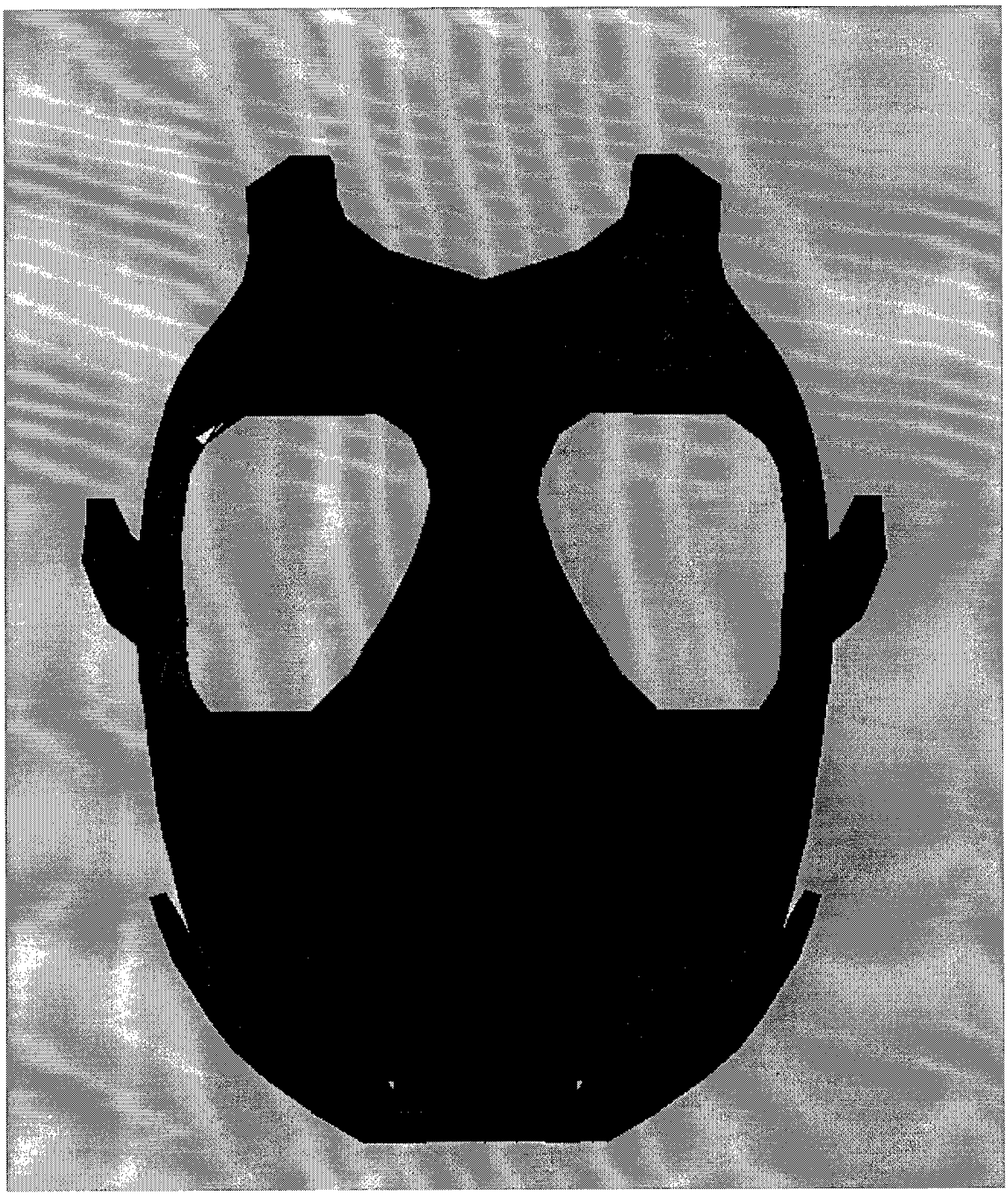

Figure 22. M40 AutoCAD Rendering

6.0 A mask fit and discomfort model

As a result of the basic efforts that are described above, a preliminary mask fit and discomfort model has been developed. This model can be seen in figure 23.

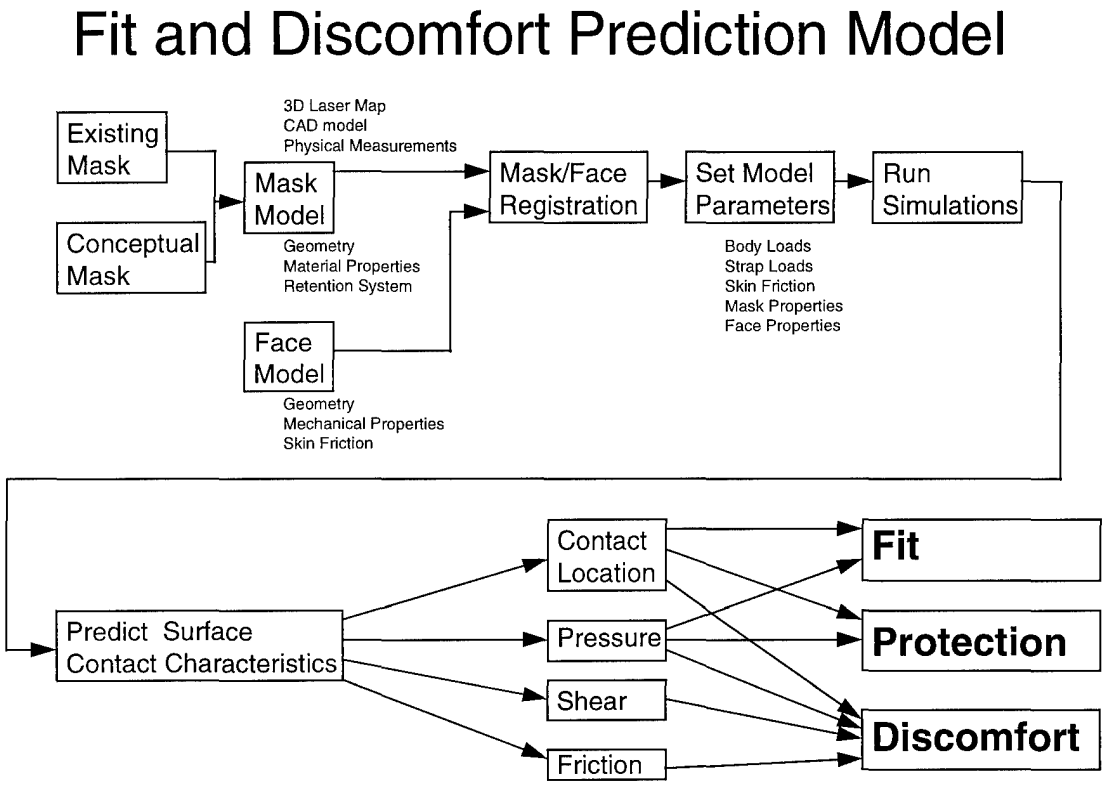

Figure 23.

The model begins with either an existing mask (such as the M40) or a conceptual mask design. A digital model of the mask must then be created using either the CAD representation of the file (if the mask was designed using this tool, a 3D laser map of the mask surfaces, or a set of measurements from the mask or a set of drawings. The mask model should be complete enough so that the surface geometry, thickness of the material, and properties of materials are specified. The second element that enters the model is the model of a human face. The only reasonable source for a head/face model is from a laser scan using a 3D mapping device. The digitized point cloud must then be treated with the appropriate software to form the complex surfaces that characterize the human face. The face model must also have appropriate mechanical properties for skin including constants for skin friction against the mask material. The two models (mask and face) are then combined in a finite element environment and the two surfaces must be registered. Once the two models are registered, an analysis of the interface can be performed. Various model parameters can be set and adjusted as required during design iterations.

Once the model parameters are set, the simulations can be run using finite element modeling (FEM) to determine surface contact characteristics. To predict fit the model must determine where the mask perimeter seal and nosecup contact the face. Fit and protection are closely related. If a mask provides the required degree of protection during tests of leakage, then the mask is said to fit. If the wearer does not complain of discomfort the mask is said to complete the criteria for fit according to persons contacted at ERDEC (C. Grove, Personal communications, December 3, 1996). The initial fit process must make sure that the seal does not contact facial hair, and that it solidly contacts the chin. There are general guidelines concerning the location of the seal with respect to the ear and forehead. The mask registration process during FEM will define the location of the contact area between the face and the mask. The contact location can be inspected using graphical depictions of the interface.

The FEM excels at determining the contact pressures of the seal against the face and the configuration of the seal. If the contact pressure is insufficient to form a seal or there is no contact between the surfaces there is potential leakage. The FEM can also calculate shear and friction that is being generated by the mask components.

To evaluate discomfort will require the integration of several of the elements discussed above. The primary determinant of discomfort for a mask wearer is pressure. As has been discussed, pressure can be calculated using this model when the mask is registered to a face. The information is available to correlate pressure on skin with tissue damage. Pain is caused by tissue damage. Data relating discomfort (in the absence of tissue damage) to pressure is not available. Since various regions of the face are more sensitive to pressure the model can alert the analyst to any pressure point that exceeds the 1.35 psi threshold that was found to cause cell change. Pressures on the nose that exceed this pressure value should be the basis for another iteration for the design. Shear can also be calculated. The most appropriate way to integrate shear forces into the model is to sum shear forces with pressure with the weighting that a unit of pressure is equal to 2.6 units of shear. While shear will probably not be a major contributor to discomfort, it may play a part in marginal situations. Friction can be generated by the FEM and is an input to the model, however, the effects due to friction from vibration or a third member such as a helmet cannot be modeled at this time.

7.0 Recommendations

The DCS team working on this Phase I SBIR has expended a significant effort to accomplish as much as possible during the term of this program. We have completed the literature reviews in the areas related to mask fit and discomfort, laser scanning, availability of software tools related to mask design, and finite element analysis. We have demonstrated the ability to use scanned images of a face and the critical elements of a protective mask in a finite element model. The FEA model has produced analytical results that were similar to those captured in an experimental setting by the sponsoring agency. The literature search in the area of discomfort has concluded that sufficient quantitative data is on hand to model the conditions that would lead to tissue damage, and therefore pain. The generation of a CAD

file of the M40 mask has utilized the scanned 3D image of the seal and nosecup. The Phase I efforts have pointed toward the need for a software design tool that merges scanning technology with FEA and CAD, as well as the need for an expert system to aid in the design process and interpret the FEA results.

A major point to be made is that the Burgess study of mask seal forces discussed in section 2.1 required three experimenters, three test items in the form of prototype masks, twelve college students, and 108 hours of data collection time. The total cost in staff hours, equipment, facilities, and elapsed time to perform the study was not documented. A potential benefit of this Phase I SBIR is to develop a method during Phase II by which this same type of study is replicated at a small fraction of the time and cost. A library of scanned faces could replace the college students, one designer could perform the entire task, and the finite element analysis may determine the seal contact forces and leakage areas in approximately 15 minutes for each mask/face combination. The use of CAD might replace the need to build a physical prototype with its attendant costs and time consumption. Software development could allow much more rapid prototype testing in a virtual environment with test results that would apply immediately to the next design iteration. The designer interface with the software could allow the performance of design functions on existing or new respirators. The respirator design could be mated to a model of a human face and an analysis of the interface might be performed. The analysis could be performed on an iterative basis using a library of face models representing the range of faces and heads in the user population. Similarly, for a given configuration of a mask, the analysis can be reiterated with varying characteristics for the properties of materials. The system output would be a representation of the new design, a set of analyses of the interface between the mask and face(s), and a set of advisories on the fit, discomfort, and other aspects of the mask design.

References

Altair Computing, (1996). HYPERMESH 2.0, Troy Michigan.

Allaire, P.E., Thacker, J.G., Edlich, R.F., Rodeheaver, G.J., and Edgerton, M.T. (1977). "Finite Deformation for *in vivo* Human Skin", J. Bioengineering, Vol. 1: 239-249.

Bader, D.L., Barnhill, R.L., & Ryan, T.J. (1986). Effect of externally applied skin surface forces on tissue vasculature. Archives of Physical Medicine and Rehabilitation, (67) November, 807-811.

Beecher, R.M. (1986). Computer graphics and shape diagnostics. Proceedings of the Human Factors Society-30th Annual Meeting (pp. 211-215). Santa Monica, CA: Human Factors Society.

Bennett, L., Kavner, D., Lee, B., & Trainor, F. (1979). Shear vs pressure as causative factors in skin blood flow occlusion. Archives of Physical Medicine and Rehabilitation, (60) July, 309-314.

Bhatia, G.H., Fiehler, G., Smith, K.E., Commean, P.K., & Vannier, M.W. (1994). A practical surface patch registration technique. Proceedings of the SPIE-The International Society for Optical Engineering (pp. 135-146). Bellingham, WA: SPIE.

Bitterman, B.H. (1991). "Application of Finite Element Modeling and Analysis to the Design of Positive Pressure Oxygen Masks", Master Thesis, Air Force Institute of Technology, Wright-Patterson Air Force Base, OH.

Blatz, P., Chu, B.M., and Wayland, H. (1969). "On the Mechanical Behavior of Elastic Animal Tissue", Trans. Soc. Theol., Vol 13: 83-102.

Burgess, W.A., Hinds, W.C., & Snook, S.H. (1970). Performance and acceptance of respirator facial seals. Ergonomics, 13 (4), 455-464.

Case, H., & Erving, C. (1989). Anthropometry of a fit test sample used in evaluating the current and improved MCU-2/P masks (AAMRL-TR-89-009). Wright-Patterson Air Force Base, OH: Armstrong Aerospace Medical Research Laboratory.

Coblentz, A., Mollard, R., & Ignazi, G. (1991). Three-dimensional face shape analysis of French adults, and its application to the design of protective equipment. Ergonomics, 34(4), 497-517.

Cohen, K.S. (1996). [Pressure along the seal for passing protection factor (16670)]. Unpublished raw data.

Coren, S., & Ward, L.M. (1989). Sensation and perception (3rd ed.). San diego, CA: Harcourt Brace Jovanovich.

Crew Technology Division of Armstrong Laboratory (1996). AAOM: Development of oxygen mask using surface scanning and rapid prototyping. Author. Available: http://www.al.wpafb.af.mil/cardlab/oxygen_masks.html.

Crisp, J.D.C. (1972). "Properties of Tendon and Skin", in Y.C. Fung, N. Perone, and M. Anliker (Eds.), Biomechanics: Its Foundations and Objectives, Prentice Hall, In., Englewood Cliffs, New Jersey, Chap. 6.

Crutchfield, C.D. (1993). Identification and review of technologies for gas mask leak detection (HEG-0006Z). Orlando, FL: NTSC R&D.

Danielson, D.A. (1973). Human skin as an elastic membrane. Journal of Biomechanics, v.6, 539-546.

Decker, R.C. and Piccione, D. (1982). Development Test II: Prototype Qualification Test - Government (POT-G) of XM33 Protective Mask, Hood, and Combat Spectacles (TECOM Report No. 8-EI-820-029-004). Fort Rucker, Alabama: U.S. Army Aviation Development Test Activity.

Demiray, H. (1972). "A Note on the Elasticity of Biological Tissues", J. Biomechanics, Vol. 5: 309-311.

Deng, Xiao Q. (1988). A Finite Element Analysis of Surgery of the Human Facial Tissues. Unpublished doctoral dissertation, Columbia University, New York, NY.

Dinsdale, S. (1974). Decubitus ulcers: role of pressure and friction in causation. Archives of Physical Medicine and Rehabilitation, (45) April, 147-152.

Dow Corning Data Sheet, Technical Information, Silastic TR-55 AND TR-70 Silicone Rubber, Dow Corning STI.

Drugge, R.J. (1996). Dermatologic terminology. [On-line]. Available: http://www.telemedicine.org/terms.htm.

Dyck, P.J., Zimmerman, I., Gillen, D.A., & Johnson, D. (1993). Cool, warm, and heat-pain detection thresholds: Testing methods and inferences about anatomic distribbution of receptors. Neurology 43(8), 1500-1508.

Fung, Y.C. (1972). "Stress-Strain-History Relations of Soft Tissues in Simple Elongation", in Y.C. Fung, N. Perrone, and M. Anliker (Eds.), Biomechanics: its Foundations and Objectives, prentice Hall, In., Englewood Cliffs, New Jersey, Chap. 7.

Fung, Y.C. (1973). "Biorheology of Soft Tissues", Biorheology, Vol. 10: 139-155.

Fung, Y.C. (1993). Biomechanics: Mechanical Properties of Living Tissue, Springer-Verlag, New York.

Geisen, G.R., Mason, C.P., Houston, V.L., Whitestone, J.J., McQuinston, B.K., & Beattie, A.C. (1995). Automatic detection, identification, and registration of anatomical landmarks. Proceedings of the Human Factors and Ergonomics Society 39th Annual Meeting (pp. 750-753). Santa Monica, CA: Human Factors and Ergonomics Society.

Gibson, T., and Kenedi, R.M. (1967). "Biomechanical Properties of Skin", Surg. Clin. North Am., Vol 47: 279-294.

Gordon, C.C., Churchill, T., Clauser, C.E., Bradtmiller, B., McConville, J.T., Tebbetts, I., Walker, R.A. (1989). 1988 Anthropometric survey of U.S. Army personnel: Methods and summary statistics. Technical Report Natick/TR-89/044, U.S. Army Natick Research, Development and Engineering Center, Natick, MA.

Gou, P.F. (1970). "Strain Energy Function for Biological Tissues", J. Biomechanics, Vol. 3: 547-550.

Green, A.E., Zerna, W. "Theoretical Elasticity, Oxford Press, 1968.

Green, B.G. (1985). Heat pain thresholds in the oral-facial region. Perception and Psychophysics, 38(2), 110-114.

Hamilton, B.E., Folds, D., & Simmons, R.R. (1982). Performance impact of current United States and United Kingdom aircrew chemical defense ensembles. Ft. Rucker, AL: U.S. Army Aeromedical Research Laboratory. (DTIC No. AD A121502).

Harrah, D. (1996). Private Communication, U.S. Army Human Research and Engineering Directorate, Aberdeen Proving Ground, MD.

Hidson, D.J. (1984). Computer-aided design of a respirator facepiece model (Report 902). Ottawa, Canada: Defence Research Establishment Ottawa.

Kenedi, R.M (1970). "The Mechanical Characteristics of Skin and Other Soft Tissue and Their Modelling", Symp. on Biodynamic Models and Their Applications, Wright-Patterson Air Force Base, Ohio, No. 12.

Kenedi, R.M., Gibson, T., Evans, J.H., and Barbenel, J. C. (1975). "Tissue Mechanics", Phys. Med Biol., Vol 20: No. 5; 699-717.

Knox, F.S., Nagel, G.A., Hamilton, B.E., Olazabal, R.P., & Kimball, K.A. (1982). Physiological impact of wearing aircrew chemical defense protective ensembles while flying

the UH-1H in hot weather. Ft. Rucker, AL: U.S. Army Aeromedical Research Laboratory. (DTIC No. AD A121581).

Kosiak, M. (1960). Etiology of decubitus ulcers. Archives of Physical Medicine and Rehabilitation, January, 19-29.

Lanir,Y., and Fung, Y.C. (1974). "Two-Dimensional Mechanical Properties of Rabbit Skin-II. Experimental Results", J Biomechanics, Vol 7: 171-182.

Lanir, Y. (1987). "Skin Mechanics", in R. Skalak, and S. Cheng (Eds.), Bioengineering Handbook, McGraw-Hill Book Company, Inc., New York, Chap. 11.

Leuder, R.K. (1983). Seat comfort: A review of the construct in the office environment. Human Factors, 25(6), 701-711.

Loveland, K., & Morrisette, J. W. (1989). Human factors in protective mask design: Literature review (Draft Report). Ft. Rucker, AL: Essex Corporation.

Manschot, J.F., and Brakkee, A.J.M. (1986a). "The Measurement and Modelling of the Mechanical Properties of Human Skin *in vivo*-I. The Measurement", J.Biomechanics, Vol. 19, No.7 : 511-515.

Manschot, J.F., and Brakkee, A.J.M. (1986b). "The Measurement and Modelling of the Mechanical Properties of Human Skin *in vivo*-II. The Measurement", J.Biomechanics, Vol. 7, No. 7 : 517-521.

Merskey, H., & Bogduk, N. (1994). Classification of Chronic Pain. International Association for the Study of Pain, IASP press, Seattle.

Mitchell, G., Knox, F., Edwards, R., Schrimsher, R., Siering, G., Stone, L., Taylor, P. (1986). Microclimate cooling and the aircrew chemical defense ensemble. USAARL Report No. 86-12. Ft. Rucker, AL: U.S. Army Aeromedical Research Laboratory.

Morrisette, J. W., & Paicopolis, P. (1991). Human factors in protective mask design: Design handbook (Draft Report). Aberdeen Proving Ground: U.S. Army Human Engineering Laboratory.

Neumann, P.F., & Sadler, L.L. (1996). Visualization package for laser scanned 3D geometry. [On-line]. Available: http://www.bvis.uic/bvl/lego/.

Ochs, J. (1992). Automated custom-fit production (AL-SR-1992-0007). Wright-Patterson Air Force Base, OH: Armstrong Aerospace Medical Research Laboratory.

Respiratory protective devices. 42 CFR 84. Code of federal regulations. Available: http://www.cdc.gov/niosh/pt84abs2.html.

Robinette, K.M. (1993). Fit testing as a helmet development tool. Proceedings of the Human Factors Society-30th Annual Meeting (pp. 69-73). Santa Monica, CA: Human Factors Society.

Robinette, K.M., & Whitestone, J.J. (1992). Methods for characterizing the human head for the design of helmets (AL-TR-192-0061). Wright-Patterson Air Force Base, OH: Armstrong Aerospace Medical Research Laboratory.

Rollman, G.B. (1991). Pain responsiveness. In Heller, M.A., & Schiff, W. (Eds.), The psychology of touch. Majwah, NJ: Lawrence Earlbaum Associates pp. 91-118.

Schiffman, H.R. (1990). Sensation and perception: An integrated approach. New York, NY: John Wiley and Sons, pp. 126-153.

Schubert, V., & Heraud, J. (1994). The effects of pressure and shear on skin microcirculation in elderly stroke patients lying in supine or semi-recumbent positions. Age and Ageing, 23, 405-410.

Silver, F.H., and Deillon, C.J. (1987a). "Skin: Structure-Mechanical Property Relationships", Biomechanics Symposium, ASME Appl. Mech., Bioeng., and Flu. Eng. conf., Cincinnati, Ohio.

Snook, S. H., Hinds, W.C., & Burgess, W.A. (1966). Respirator comfort: subjective response to force applied to the face. American Industrial Hygiene Association Journal, March 93-97.

Snyder, R.W., and Lee, L. H.. N. (1975). "Experimental Study of Biological Tissue Subjected to Pure Shear", J. Biomechanics, Vol. 8: 415-419.

Thacker, J.G., Stalnecker, M.C., Allaire, P.E., Edgerton, M.T., Rodeheaver, G.T., Edlich, R.F. (1977b). "Practical Application of Skin Biomechanics", Clinics in Plastic Surgery, Vol.4, No.2 : 167-171.

Tong, P., and Fung, Y.C. (1976). "The Stress-Strain Relationship for the Skin", J. Biomechanics, Vol. 9: 649-657.

Vannier, Michael W., Yates, Ronald E., & Whitestone, Jennifer. J. (Eds.). (1992). Electronic Imaging of the Human Body Workshop. Dayton, OH: Crew System Ergonomics Information Analysis Center.

Veronda, D.R., and Westmann, R.A. (1977). "Mechanical Characterization of Skin-Finite Deformations", J. Biomechanics, Vol. 3: 111-124.

Whirley, R.G., & Engelmann, B.E. (1993). DYNA3D, UCRL-MA-107254, Lawrence Livermore National Laboratory.

Whitestone, J.J. (1991). Human factors in design and evaluation of helmet systems: An overview. Proceedings of the Human Factors Society-30th Annual Meeting (pp. 63). Santa Monica, CA: Human Factors Society.

Whitestone, J.J. (1993). Design and evaluation of helmet systems using 3D data. Proceedings of the Human Factors Society-30th Annual Meeting (pp. 64-68). Santa Monica, CA: Human Factors Society.

Whitestone, J. J., & Robinette, K.M. (1996). Fitting to maximize performance of HMD systems. In Head-mounted displays: Designing for the User [On-line]. Available http://www.wpafb.al.af.mil/cardlab/publications.html.

Xakellis, George C., Franz, Rita A., Arteaga, Manuel, & Meletiou, Steve (1993). Dermal blood flow response to constant pressure in healthy older and younger subjects. Journal of Gerontology, 48, M6-M9.

Zehner, G.F. (1986). Three-dimensional summarization of face shape. Proceedings of the Human Factors Society-30th Annual Meeting (pp. 206-210). Santa Monica, CA: Human Factors Society.

Zhang, L., Helander, M.G., & Drury, C.G. (1996). Identifying factors of comfort and discomfort in sitting. Human Factors, 38(3), 377-389.